Icarus 320 (2019) 159–187

Contents lists available at ScienceDirect

Icarus

journal homepage: www.elsevier.com/locate/icarus

The central pit and dome at Cerealia Facula bright deposit and floor deposits in Occator crater, Ceres: Morphology, comparisons and formation

Paul Schenk*, Hanna Sizemore, Britney Schmidt, Julie Castillo-Rogez, Maria De Sanctis, Timothy Bowling, Jennifer Scully, Debra Buczkowski, Lynnae Quick, Frank Preusker, Ryan Park, Carol Raymond, Chris Russell, the Dawn Science Team

LPI, Houston, TX, USA

A B S T R A C T

The prominent bright deposit Cerealia Facula, Ceres, coincides with the central depression (or central pit) of the recently formed 92 km-wide complex crater Occator. The central pit is 9–10 km wide and up to 1 km deep and is partially filled with a 700 m-high 2 km-wide dome. The upper surface of the central dome is densely fractured but the flanks are not, indicating that uplift of the dome surface occurred after the bright deposit was emplaced, and primarily through uplift of the surface from below by laccolithic intrusion or volume expansion. The pit is rimless except for two prominent massifs that flank it to the east and west. This pit-dome morphology bears a strong resemblance in morphology, topography, and dimensions to central pit craters observed on Ganymede and Callisto, but is essentially absent on the similar sized ice-rich moons of Uranus, Saturn, and Pluto. The lack of pit craters on midsize icy moons and the possible lack of central pit craters at the cold poles of Ceres suggest that temperature is a significant controlling factor in central pit formation, beyond the canonical inverse-gravity scaling of complex crater transitions. While renewed modeling will benefit from these new constraints, the mapping of central pits on Ceres, including Occator, suggests that either the rheologically layered target model or more likely the melted central uplift model may be the most probable explanation for central pit formation on Ceres (lack of similar high-resolution imaging on the Galilean icy satellites precludes definitive evaluation of models there). Large volumes of lobate floor-fill material at least 600 m thick in some places cover large areas of the southern and eastern floor of Occator, and small outcrops of this unit are found perched high on closed topographic depressions on the Occator terrace zone and other higher areas of the crater floor. The swirling and knobby surface textures of these lobate deposits are essentially indistinguishable from those on impact melt sheets on large lunar craters such as Tycho. These observations indicate that this unit is most likely an impact melt sheet formed from melted water ice admixed with unmelted particulate or dissolved phyllosilicates, salts and/or carbonates, and large quantities of fragmented debris. Melt of ice phases within Ceres crust is also supported by independent numerical models of impact at Occator and would provide a ready source of fluids to promote hydrothermal deposition of the observed bright Na-carbonates on the surface of the central pit at Occator, if the deposit formed within a million years or so of impact. The central dome finds analogs in salt domes on Earth and pingos (frost-mounds) on Earth and Mars, which form by water and solute migration and freeze expansion. Later freezing of a central reservoir of volatiles beneath the central pit at Occator or mobilization of ice or other phases during the cooling and refreezing process could explain the uplift of the central dome. Finally, no changes were detected in the Cerealia and Vinalia Facula bright deposits during the course of the prime Dawn mapping mission, placing additional constraints on their formation time and limits on ongoing activity.

1. Introduction

Dwarf planet Ceres, as the largest current member of the Asteroid Belt, is noteworthy for its low density of ~2.16 g/cm^3 indicating a water content of ~50 vol.% in the form of ice and water of hydration (silicates and salts) (e.g., McCord and Sotin, 2005). Modeling based on global geophysical mapping of Ceres by the Dawn spacecraft indicates that it may be only weakly differentiated and that the outer layers may have no more than 40% water ice (Bland et al., 2016; Park et al., 2016; Fu et al. 2017). Despite this, global mapping by Dawn (Russell et al., 2016) has revealed a variety of geologic features indicative of low-strength or ice-rich materials in the outer layers, including debris slides (Schmidt et al., 2017), volcanic domes (Ruesch et al., 2016; Sori et al., 2017), impact crater transition diameters identical to icy satellites (Hiesinger et al., 2016; Schenk et al., 2016), and other related features (e.g., Sizemore et al., 2017).

The first anomalous features discovered in the early stages of Dawn Ceres mapping were bright spots (Fig. 1) on the floor of a large relatively fresh 92 km-wide impact crater (Occator) in one of the regions originally thought to be venting water (Kueppers et al. 2014). These spots, or faculae, are the brightest features on the planet and spectroscopy revealed a composition dominated by Na-carbonates, Al-phyllosilicates and NH_4CL (De Sanctis et al., 2016; Raponi et al., 2018, this issue). Higher resolution images revealed the brightest and largest spot, named Cerealia Facula, to be coincident with a depression (or pit) and small dome at the center of Occator crater. Central pits turn out to be

* Corresponding author.
E-mail address: schenk@lpi.usra.edu (P. Schenk).

https://doi.org/10.1016/j.icarus.2018.08.010
Received 27 December 2017; Received in revised form 23 June 2018; Accepted 15 August 2018
Available online 19 August 2018
0019-1035/

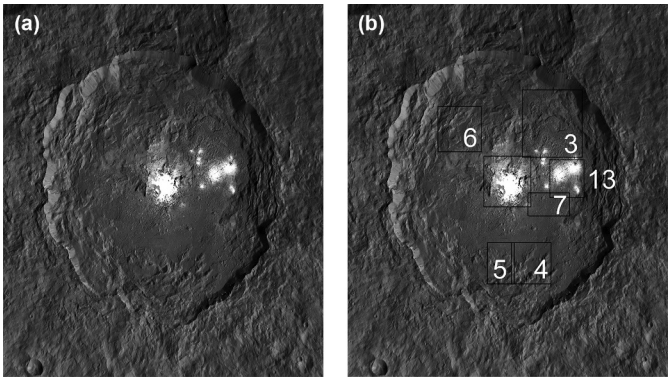

Fig. 1. (a) Occator crater, Ceres. Image is from global base mosaic at ~35 m pixel scale. Crater is 92 km across; north is at top. Bright deposits are saturated in this view but are presented more naturally in subsequent figures. (b). Version of Fig. 1 with annotation showing approximate locations (boxes) of other figures illustrating features within Occator crater. The center square shows the approximate location of Fig., 8–12, and 20.

common in large craters of this size on Ceres (Schenk et al., 2016) and an understanding of the formation of these central structures is one of the fundamental keys to unlocking the origin(s) of this unusual bright feature.

In this report we examine the morphology of the Occator central structure and compare it with similar central structures on Ceres and on icy satellites. We also examine surrounding features within Occator to place the central structure in context. We then examine constraints that the occurrence of these structures on Ceres place on central pit formation generally and what their formation implies for the state of Ceres' interior.

2. Occator Crater: description

Global mapping of Ceres and stereo and visible-NIR imaging of Occator in particular were acquired by Dawn at pixel scales of ~35 m/pixel, supplemented by IR spectroscopy (e.g., Ammannito et al., 2016; Carrozzo et al., 2018; Ciarniello et al., 2017; Nathues et al., 2016). Stereo imaging allowed for detailed topographic mapping (Fig. 2) in both stereogrammetry (Preusker et al., 2016) and stereophotoclinometry (Park et al., 2016) supplemented by individual DEM (digital elevation models) construction by the author (PS) over the central structure of Occator. The features described here are based on mapping at ~35 m pixel scales, supplemented by stereo views and DEM data.

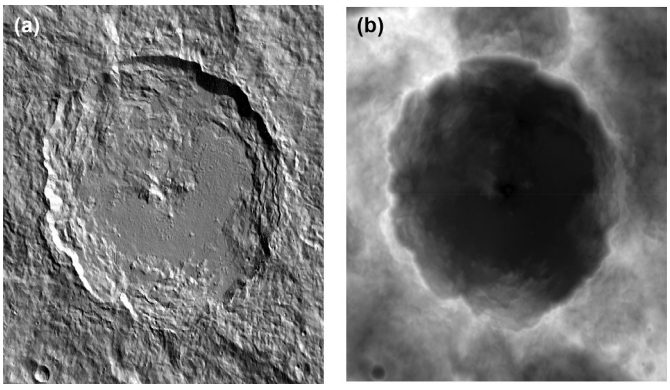

Fig. 2. (a) Stereogrammetric topographic map of Occator crater, Ceres (Preusker et al., 2016). Image is from global DEM at ~35 m pixel scale. Crater is 92 km across; north is at top. (b) Shaded relief rendering of DEM shown in Fig. 2a. Artificial illumination is from upper right, highlighting the relief in the central region.

The geology of Occator is described in greater detail by Buczkowski et al. (2017, this issue) and Scully et al. (2018, this issue) and is addressed here in brief as context for the examination of the central structure. As we are concerned here primarily with the central bright deposits and structures of Occator, we defer discussion of ejecta deposits to other reports (e.g., Buczkowski et al., 2017 this issue; Scully et al., 2018, this issue; Nathues et al., 2018, this issue) except to note them as evidence of impact origin.

Occator crater (19N, 239E) is a nearly circular rimmed depression 93 by 89 km across and ~3.75 km deep (Figs. 1 and 2). Occator is the largest well-preserved crater and is the only one >75 km across on Ceres where all original structures and textures from formation are reasonably intact, at 35 m resolutions. The current estimated age of formation of the Occator crater is ~20 Myr (Neesemann et al., 2018, to this issue). We note that there is variability and uncertainty in the estimates of areas within the crater due to small area stochastic cratering variability and likely contamination of self-secondaries in the counts which will make reliable estimates of smaller areas very difficult. The crater is defined by a steep inward-facing scarp bounding a rugged but low lying floor of ridged, hummocky, and flat-lying materials (e.g., Scully et al., 2018, this issue). The crater itself is surrounded by heavily scoured and mantled terrains and fields of innumerable irregularly shaped craters, consistent with formation of a large impact crater surrounded by ejecta deposits and secondaries, though these are not addressed in this report.

2.1. Rim morphology and floor Units

The rim scarp of the Occator basin rises an average of 3.75 km above the crater floor and has slopes of 30–50° (Fig. 1). The height of the wall scarp is variable (Figs. 1 and 2). In some areas, particularly to the northeast and southeast, the wall scarp drops precipitously in one contiguous scarp several kilometers to crater floor deposits. In other areas the rim wall scarp is less tall, particularly where the crater floor deposits are higher in elevation and presumably thicker. Small rugged km-scale knobs are locally exposed along the crest of the rim scarp (Fig. 3a[*left*]) inferred to be exposures of bedrock or strongly consolidated crustal materials. Some of these spots are relatively bright in contrast to other materials. Otherwise the slopes of the rim wall are mostly smooth with downslope light-and-dark striations (Fig. 3a) suggestive of loose unconsolidated talus debris, or normal fault scarp formation, or both. Individual debris slides outlined by lobate distal margins are recognized along the base of this wall, though these are volumetrically negligible, compared to crater volume.

The floor of the basin is comprised of three main geomorphic units (Buczkowski et al., submitted this issue; Scully et al., submitted this issue). The outermost unit, located along the base of the wall scarp, is the terrace material, consisting of a circumferential zone or wreath of uneven hummocky material and angular arcuate blocks of variable shape up to 10 km across and 1–2 km high (Fig. 3a). These blocks are not as discrete and well organized as in some larger lunar craters but are nonetheless recognizable in many areas as tilted fault blocks. In a few locations the scarps defining these smaller blocks bifurcate, consistent with formation of nested terrace scarps.

Interior to the terrace zone lie two distinctly different major floor units. Most of the northwest half of the crater floor is comprised of the hummocky floor unit, consisting of irregular mounds and ridges with uneven topography (Figs. 1–3). This hummocky floor unit blends laterally with the more organized terraced material proximal to the wall scarp and is sometimes difficult to distinguish as a discrete unit. These units are interpreted as fractured crater floor material disrupted and displaced due to rim wall slumping and floor uplift associated directly with the Occator impact event.

The southeastern half of the crater floor (Buczkowski et al., 2017, this issue; Scully et al., 2018, this issue) is dominated by a nearly flat-lying "lobate" floor-filling deposit (Figs. 1 and 3) that locally embays

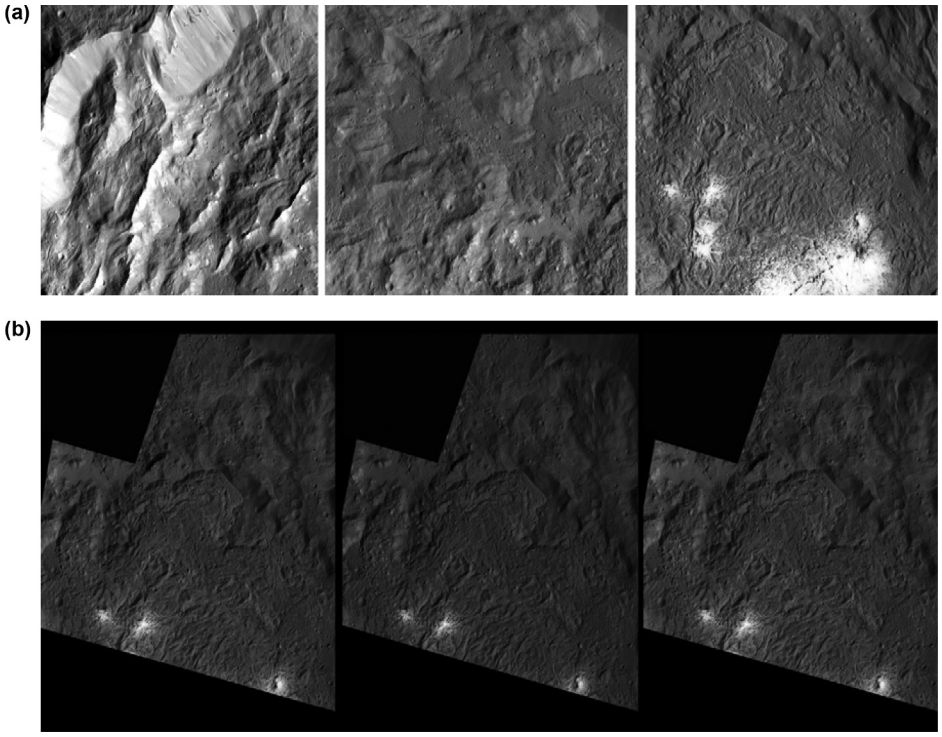

Fig. 3. (a) Major floor unit types within Occator impact crater. From left to right: wall scarp and terrace zone; hummocky floor unit; lobate floor-fill unit. Scene widths are ~35 km; north is at top. Images were acquired at pixel scales of ~35 m. (b) Stereographic view of northern outcrops of ridged and knobby lobate floor-fill material of Occator crater. Lobate deposits are in central third of scene, uncovered hummocky floor deposits in top third of scene. Several bright spots of Vinalia Facula (described below) are visible. Images were acquired at pixel scales of ~35 m. Figure format allows user to view in either wall-eyed model (left-center) or cross-eyed mode (center-right).

low-lying parts of the rim terrace unit and irregular hummocky floor unit. The main contiguous exposure of this smooth embayed unit covers ~1/3rd of the floor and forms a large U-shaped deposit opening to the northwest and surrounding the central complex (Fig. 2). While rugged on kilometer scales (Fig. 3), this unit is remarkably flat-lying in the elevation map (Fig. 2), with local relief rarely exceeding 100 m. Despite this, the unit is not flat-lying on a regional scale, with a gentle rise of ~500 m forming the western section (Fig. 2). This lateral asymmetry in the distribution of the lobate material suggests possible oblique impact from the SE or NW, but could also indicate impact into a target with lateral preexisting variations in composition or topography. Indeed, the embayment of terraces in the southeast quadrant also suggests that the hummocky and terraced crater floor material beneath the lobate deposit is generally lower to the southeast than to the northwest.

The distribution and morphology of lobate floor-fill material is complex. Except in the southeast, the bulk of the lobate material lies interior to the terraced units. Along the southeast rim the lobate floor-fill materials extend up to the base of the wall scarp and embay terrace blocks, which are lower in this quadrant (Figs. 4 and 5). Numerous smaller outcropping of this unit can be identified within the terrace zone, and within the hummocky floor material (Figs. 4–6). These smaller units mostly lie in shallow topographically isolated depressions at different elevations on the crests of terrace blocks or between ridges or hummocks within the crater floor unit. In numerous cases, narrow ribbons of this material can be observed draped between terraces of different elevations, with clear indications locally of narrow channelized flow downslope (Figs. 4–6) from one level to another.

In many areas, the outer margins of lobate floor-fill material abut rim wall or terrace block scarps directly with little indication of significant relief (Figs. 4 and 5). In other areas, particularly the northeast, the lobate unit has a definitive outward facing scarp with a rugged knobby and ridged surface and relief of several hundred meters (Fig. 3b). In fact, the deepest exposed terrains on the crater floor are uncovered hummocky floor units just beyond the northern edge of the lobate deposit (Figs. 2 and 3b). These morphologies are consistent with lateral flow of a material of variable viscosity emplaced in various directions.

The surface of the lobate floor-fill unit has textures that can be described variously as ropy, ridged, sinuous, knobby or hilly (Figs. 3 and 7), with local relief that only rarely exceeds a hundred meters. There is a northward gradation to more rugged relief with no resolvable break (Buczkowski et al., submitted this issue; Scully et al., submitted this issue), suggesting emplacement in one single episode. These surface textures are morphologically indistinguishable to those on impact melt sheets of large fresh lunar impact craters (Fig. 6), specifically Tycho and Copernicus. We infer (as also discussed by Scully et al., submitted this issue) based on these similarities and the embayment of terrace ridges and scarps at various elevations, that the deposits across the floor of Occator are analogous, forming a large impact melt sheet, a conclusion explored in more detail in the Discussion section.

2.2. Central pit and central dome structures

Unpublished pre-Dawn-arrival studies of impact cratering on Ceres by the authors predicted that large craters in the 10–300 km size range would have large conical central peaks, the prevalent morphology on similarly sized ice-rich Dione and Tethys (e.g., White et al., 2013, 2017), if the outer layers of Ceres were similarly ice-rich (e.g., McCord and Sotin, 2005). While smaller craters (<40 km) on Ceres are nearly indistinguishable from those on midsized Saturnian icy moons as observed by Cassini, most larger craters are central pit craters.

On Ceres, most craters between ~70 and 150 km have central pits instead of central peaks (Schenk et al., 2016; Hiesinger et al., 2016), in which rimmed shallow depressions or 'pits' replaces the rugged massifs that constitute central peaks.

The central pit of Occator is ~9 km across and ~1 km deep with respect to the crater floor (Figs. 8 and 9). The southern and northern edges of this depression are broadly convex in profile and rimless, with effective slopes of <10°. The rugged textures of the lobate floor-fill deposit continue up to the topographic edge of the pit in these sectors until the bright deposits described below obscure it. Thus it is unknown whether the pit floor is comprised of lobate floor-fill material or hummocky floor materials.

The eastern and western edges of the Occator central pit are flanked by high-standing irregularly shaped massifs that form an incomplete elevated ring around the depression (Fig. 8). The most prominent

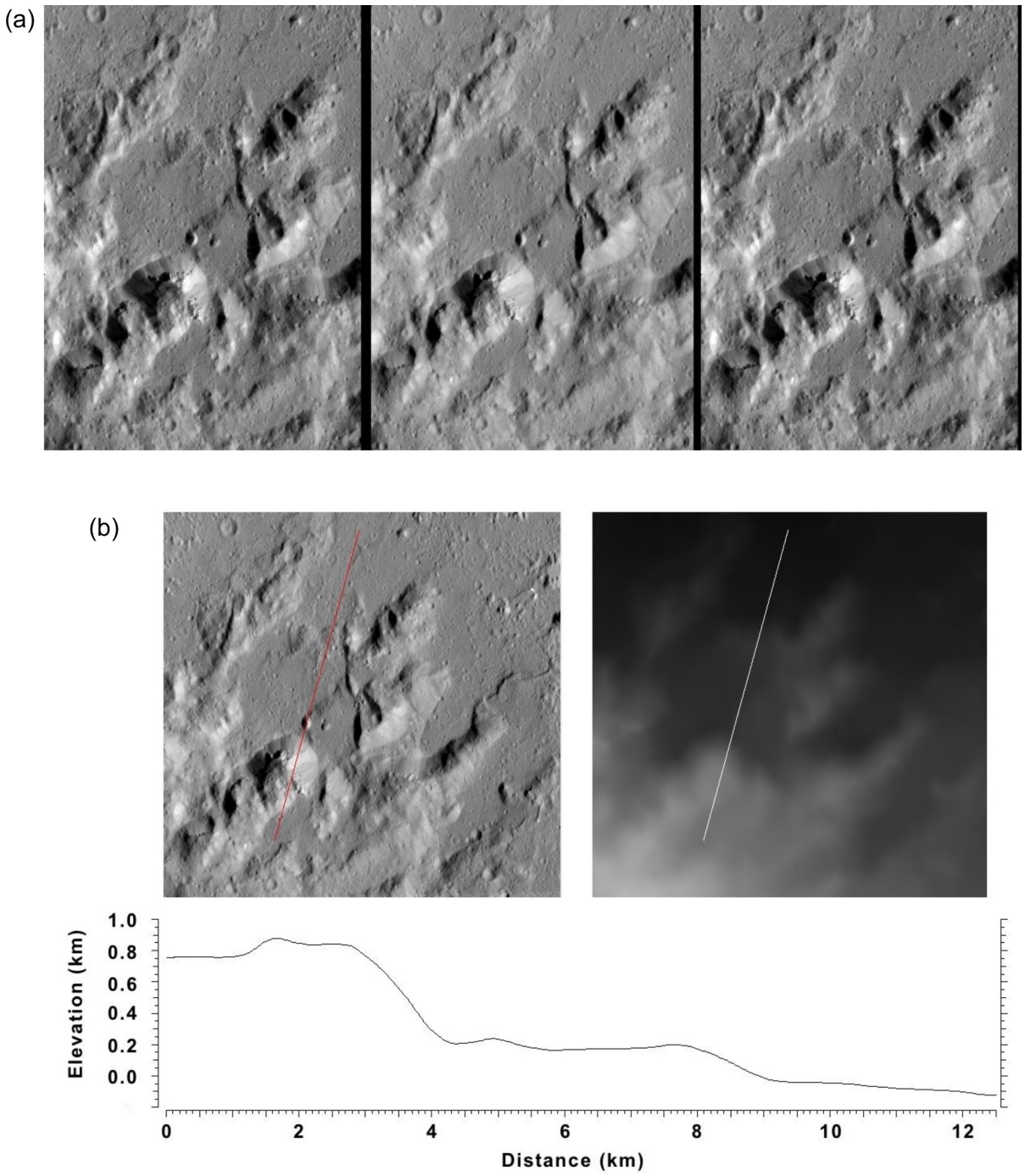

Fig. 4. (a) Stereographic view of outcrops of smooth textured floor-fill material isolated within the southern rim wall terrace zone of Occator crater. Images were acquired at pixel scales of ~35 m. Figure format allows user to view in either wall-eyed model (left-center) or cross-eyed mode (center-right). (b) Image (left), DEM (right), and topographic profile (bottom) across exposures of lobate floor-fill material shown in Fig. 4a, showing perching of lobate material at −200 m, 150 m, and 1050 m at this site.

topographic element of this partial pit rim is a polygonal massif roughly 10 km on a side on the western edge of the central depression, which rises ~2 km above the crater floor and 3 km above the depression floor (Fig. 8a). Most of this fractured plateau slopes generally away from crater center and has a surface morphology like that of the ridged and disrupted hummocky floor material to the northwest. This massif is highest adjacent to the central pit where its edge is defined by a high broken ridge forming several aligned singular massifs. The inner portion of this ridge forms a steep-walled amphitheater descending into the central pit, flanked by a smaller mesa, which extends to the south. Portions of the crater floor fracture system described below extend up to the southern rim within the lobate deposit but are not observed on the north side of the rim where hummocky floor material dominates.

The smaller massif to the east is roughly 3 × 5 km on a side and rises ~1 km above floor material (Fig. 8b). It is more irregular in shape than the western massif but appears to have a small mesa-like crest. The massif also has a deep quasi-concentric fracture cutting it in two major sections; the section of which closest to the central pit has a flat top sloping toward crater center that could be interpreted as having been rotated toward the crater during pit formation. Several smaller massifs also occur elsewhere in the annular region flanking the central pit but these are not continuous or contiguous with other elevated features and

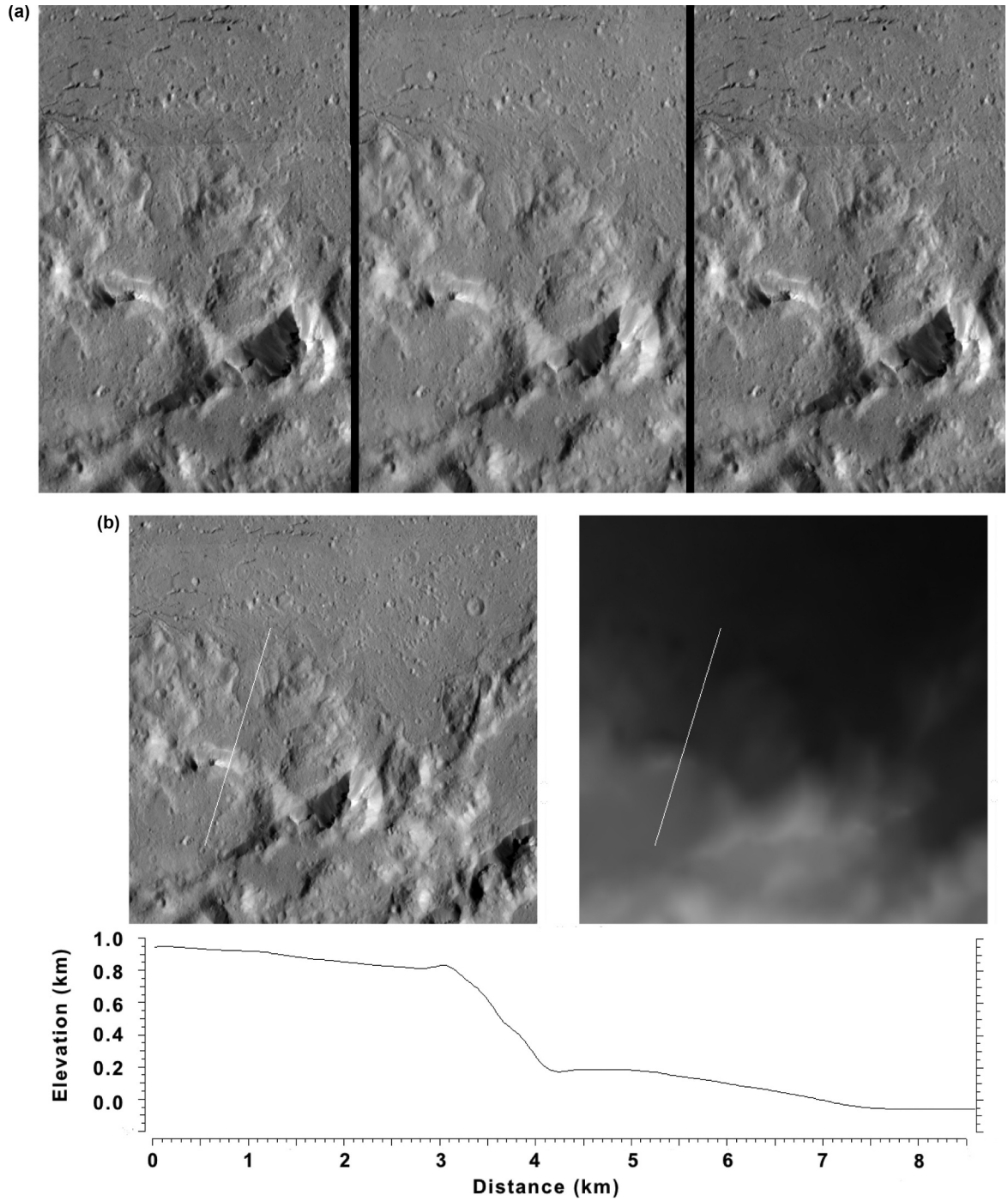

Fig. 5. (a) Stereographic view of outcrops of smooth textured floor-fill material isolated within the southern rim wall terrace zone of Occator crater (immediately due west of Fig. 4). Images were acquired at pixel scales of ~35 m. Figure format allows user to view in either wall-eyed model (left-center) or cross-eyed mode (center-right). (b) Image (left), DEM (right), and topographic profile (bottom) across exposures of lobate floor-fill material shown in Fig. 5a, showing perching of lobate material at 900 m and 0–200 m at this site, emphasizing the downward sloping surfaces of some of these units.

are less than 1 km high (Fig. 8).

Near the center of the pit lies a circular rounded dome ~3 km wide and ~750 m high (Figs. 9 and 10). The dome is slightly offset to the southeast from the deepest part of the pit. Its highest relative height above its base is ~900 m on its northwest slope (Figs. 9 and 10). At 35 m pixel scales, the dome is densely fractured in a crossing pattern on its upper surfaces, though the fractures are less intense along the flanks and with a possible exception do not extend beyond the edge of the dome into the surrounding pit walls.

Although we observe knobby material and perhaps a low scarp along the northern edges of the dome, perhaps a fracture, the southern edge of the topographic dome (at 35 m/pixel resolutions) betrays no evidence for any bounding or marginal scarp along the edge of the dome. Rather we observe a continuous transition in the bright deposit from the inward sloping pit wall onto the outward-sloping dome (Fig. 9, 11), suggesting they are formed from one contiguous geologic unit, and that the domal uplift and fracturing formed after the bright material was most in place.

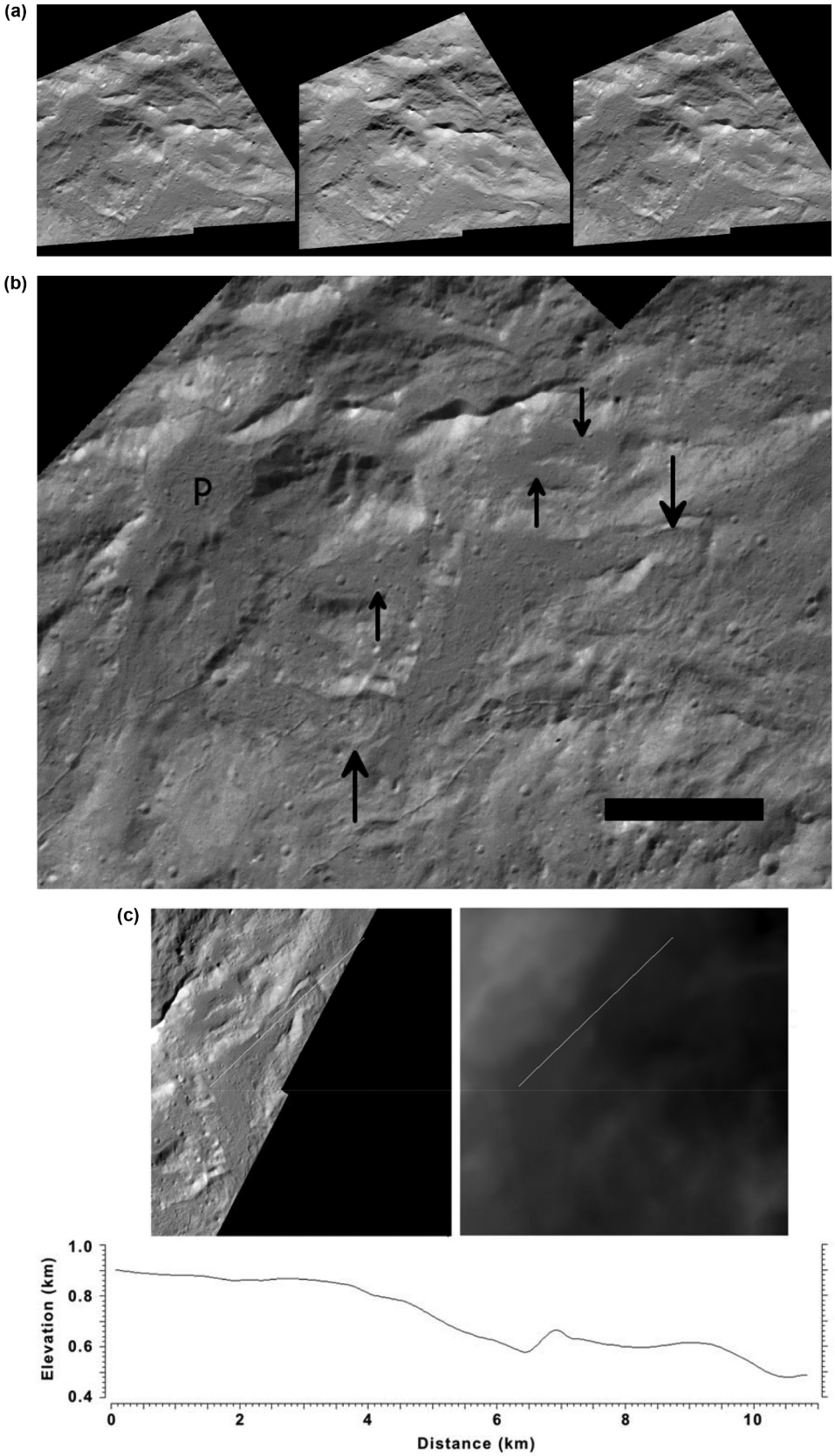

Fig. 6. (a) Stereographic view of outcrops of lobate material isolated within the northwestern hummocky floor material unit. Images were acquired at pixel scales of ~35 m. North is to the upper right. Figure format allows user to view in either wall-eyed model (left-center) or cross-eyed mode (center-right). (b) Enlarged view of stereo view in Fig. 6a showing the area is more detail, including two downslope flow lobes (large arrows), perched units of smooth material (small arrows) and ponded lobate material ~300 m wide in a closed depression (p). (c) Image (left), DEM (right), and topographic profile (bottom) across a downslope flow-like lobe of lobate floor-fill material shown in Fig. 6a, indicating at least 300 m of relief from upper flow to its snout. A second flow lobe is visible at bottom left.

2.3. *Cerealia facula bright deposit*

In addition to its Na-carbonate- and NH_4CL-rich composition (De Sanctis et al., 2016; Raponi et al., submitted this issue), the spatial distribution and stratigraphy of the bright deposits within Occator are key to understanding their emplacement. The bright deposits at Occator occur in two main exposures. The brighter Cerealia Facula (Figs. 9 and 11) is closely associated with the topographic limit of the central pit

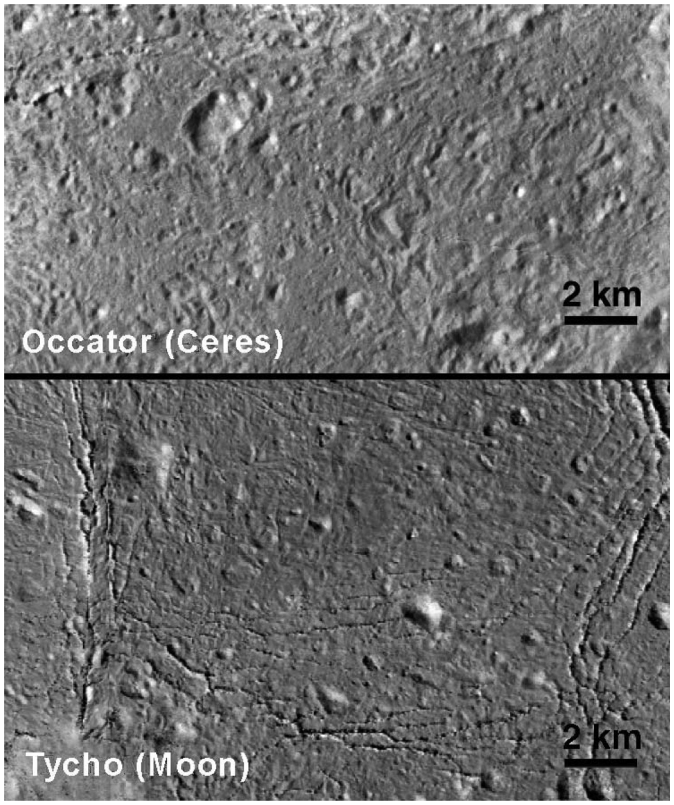

Fig. 7. Lobate floor-fill deposits on floors of Occator crater, Ceres (top) and Tycho crater, Moon. Floor of Tycho are similar in appearance to those on Occator, including swirl textures, through-going fractures (not shown in this view, see Figs. 1 or 9), low irregular mounds of similar size and shallow irregular depressions. Occator surface textures become smoother to the south of this view.

and does not extend appreciably onto the broad lobate floor-fill deposits beyond (except where lobate material overlaps onto the edge of the pit itself). These bright materials have sharp contacts (at 35 m pixel scales) with dark material within the central pit floor (Figs. 9 and 11), suggesting these are discrete material units with non-trivial thicknesses.

Not all of the surface of the central pit is covered by bright materials (Figs. 9, 11 and 12). While the lowest parts of the pit and the dome itself are completely covered by the bright deposit, the upper slopes of the outer pit walls are variably covered. Some exposures occur as narrow strands or tendrils of bright material (<1 to ~2 km wide) extending up the slopes of the pit and flanking massifs (Figs. 8 and 9) and giving the visual impression of an octopus with short arms, centered on the dome. Bright material is also visible as small discreet spots a few hundred meters or less across along the outer margins of Cerealia Facula (Figs. 9 and 11), particularly to the south and northeast.

The central dome is entirely covered by the bright deposit. Framing Camera color imaging indicates that while the bright deposit overall is redder than crater floor material, the visible color of the dome is distinctly 'reddish' within the fractures near the crest compared to unfractured dome and pit bright materials (Fig. 11). This indicates layering of some sort, with materials perhaps a few meters or 10 s of meters below the surface having a different (though still bright) color and perhaps different composition from the surface layers of the deposit.

Elsewhere, bright materials have a complex relation to topography within the central pit (Fig. 12). While the general outline of Cerealia Facula follows the outline of the central pit, at sub-kilometer scales, the edge does not and bright material can be perched well above dark material. This is especially evident in the western sector where the presence of several ribbon-like tendrils are observed 'running' downslope next to uncovered dark material (Figs. 9a and 12), including dark material on the deepest part of the central pit. As another example, several small dark spots several hundred meters across are evident within Cerealia Facula (Fig. 11). These dark spots are identified in the stereo images and DEM (Figs. 9 and 10) as knobs a few hundred meters high at most, and can have bright material on either their inward-facing or outward-facing slopes (facing relative to crater center). The small uncovered knobs within Cerealia Facula suggest that the bright material was partially controlled by local topography, flowing around or onto one side of small obstacles. Ballistic emplacement is not ruled out in some cases. On the other hand, the tendrils and small spots on the outer margins suggest origins at multiple discrete sources on the outer flanks of the central pit, with downslope flow in some areas accumulating at the base of the pit.

Bowling et al. (2018, this issue) postulate that the liquid water "melt plug" formed at the center and potentially responsible for the missing central peak (and which are observed on the mid-size icy satellites) could have ponded in the central pit long enough to precipitate carbonates and chlorides directly onto the 'lake bed.' To explain the absence of any significant water ice signatures in this area would require either complete drainage of the water after the bright deposits lined the lake bed (assuming the deposits do not seal off most drainage pathways) or sublimated into space. The most direct indication of whether such a temporal lake existed would be the contours of the bright deposit (Fig. 12). While the outline of the deposit does approximately follow the topographic contours of the pit in basic outline, the detailed trace of the edge of the deposit does not, with bright materials perched on plateaus and dark material in low areas within the pit margins. Secondary processes such as mass wasting or ballistic emplacement of solute-rich waters onto higher ground may alter the disposition of bright materials. Higher resolution images will be required to address these possibilities.

Probably the most enigmatic outcrops of bright material at Cerealia Facula are those perched on two small plateaus the large western and eastern massifs closest to the central pit (Figs. 8, 9, 11 and 12). Both plateaus rise ~2 km above the pit floor, with flanks of dark material. Faint traces of bright material can be found streaking this scarp downslope from the bright deposit outcrop at several locations (Figs. 8, 9 and 11), indicating that bright material can mix with and be darkened by substrate material on steep slopes. This mixing process might occur on other steep slopes within the central pit, complicating stratigraphic determinations. The topographically isolated bright-capped block in Fig. 9a is near the elevation of the crater floor to the south and thus is not as high as the peak massifs of the western pit rim. Formation of bright material on mesa tops could indicate ballistic "airfall" style emplacement of some bright material, uplift of covered mesa blocks after emplacement, or the presence of discrete bright material sources even on mesa crests.

Stratigraphically, then, the Cerealia Facula bright deposits must have formed after the central pit, given that undisturbed bright deposits form on the walls of the central pit, including the steeper western wall (Fig. 9). The deposits also appear to be cut by crater floor fractures described below (e.g., Buczkowski et al., submitted this issue) that flank and partly disrupt the outer central pit regions to the south. This suggests that the bright deposits also formed after the lobate floor deposits solidified but before the extensive floor fracture network formed. Here, though, the downslope mixing of dark and bright materials described above may mask post-fracturing deposition of bright material on fracture walls. These fractures form the isolated mesas along the eastern and southern edges of Cerealia Facula (Fig. 8) and can be attributed to either cooling and contraction of the floor deposits as they solidify (as at Tycho crater), or post-impact sub-floor intrusions and surface inflation (e.g., Buczkowski et al., 2017, this issue). The former would occur on the time scale of days to months depending on thickness, but the latter could occur over a longer time period (calculations specific to Ceres would be required to be more precise). Deposition of the bright

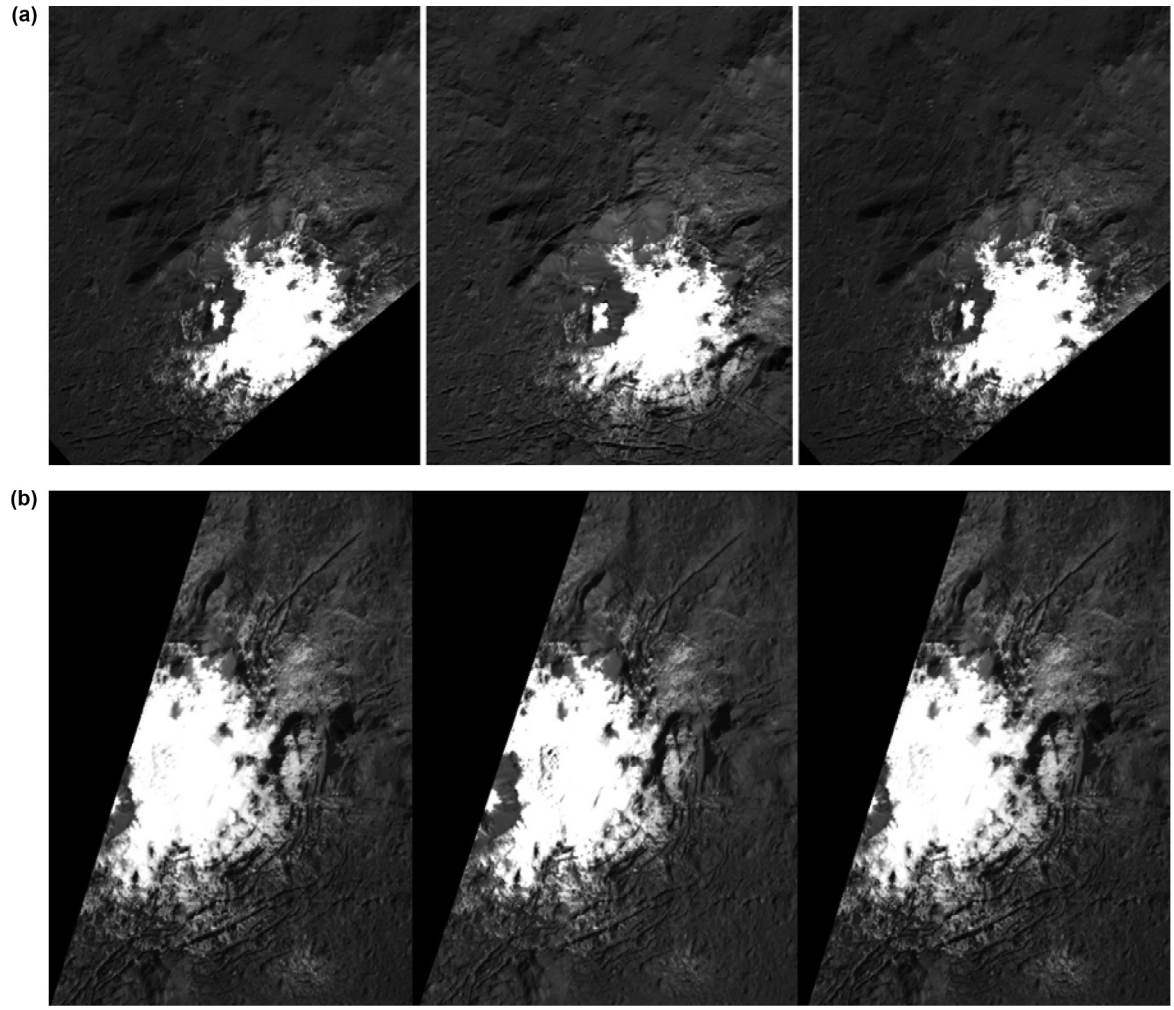

Fig. 8. (a) Stereo anaglyph of central pit and domes structures in Occator crater, centered on the western massif. Images were acquired at pixel scales of ~35 m. View is contrast stretched to emphasize the darker pit walls and crater floor; north is to upper right. Figure format allows user to view in either wall-eyed model (left-center) or cross-eyed mode (center-right). (b) Stereo anaglyph of central pit and domes structures in Occator crater, centered on the eastern massif. Images were acquired at pixel scales of ~35 m. View is contrast stretched to emphasize the darker pit walls and crater floor; north is to upper right. Figure format allows user to view in either wall-eyed model (left-center) or cross-eyed mode (center-right).

materials likely predates dome formation, as the deposit forms a contiguous cover over pit and dome that is fractured only on the dome itself.]]

Whether bright material formed immediately after the observed crater structures or after a prolonged period is more difficult to ascertain. Small randomly spaced pits are evident across the surface of the bright carbonate and NH_4CL deposit, a few of them with bright haloes (Fig. 11). Whether these are small impact events or outgassing vents is not resolvable in the Dawn images, but on the assumption these are impacts, Neesemann et al. (2018, this issue) has determined that the bright deposit has a lower crater density and could be a few million years or more younger than average crater floor and ejecta materials. Of course, the counting area is very small ($\leq$75 km^2) and this area may simply have been cratered less as a result of stochastic variability in crater density. The bright deposits, if a coherent solid "rock" formation, may also have different mechanical properties than the impact debris lining the remainder of the crater floor, possibly resulting in the formation of even smaller craters (Dundas and McEwen, 2010). Both effects indicate a larger uncertainty in the estimated age of this small deposit compared to the much larger counting area of the crater floor.

2.4. Crater floor structures and Vinalia Faculae

Discrete narrow linear and curvilinear depressions (e.g., Buczkowski et al., 2016; submitted this issue) cross the floor of Occator. Although most form within the lobate floor-fill deposit, some extend into the terrace zone and clearly postdate the impact event. The most prominent sets of fractures relevant to the central features of Occator extend from the SW wall scarp to the central structure (Fig. 1), where some form concentric rings around the southern section of the central pit. Other fractures continue on toward the east across the lobate deposits covering the eastern floor of the crater where they are spatially associated with the smaller Vinalia Faculae bright deposits in that region (Fig. 13). We note that most of the Occator floor fractures are not associated with bright deposits.

The Vinalia Faculae bright deposits in Occator form an ~20 by 25 km wide cluster of ~8 discrete small approximately circular patches located within the eastern extension of the lobate floor-fill deposit (Figs. 1 and 13). Stereo imaging reveals that the surfaces associated with these spots have very low relief of <100 m. They are not associated with any discrete edifice or depression, but may be associated with poorly resolved point sources. The two largest patches appear to be associated with a dark ring and a north-south trending fissure, respectively, whereas at least two of the smaller patches appear to have

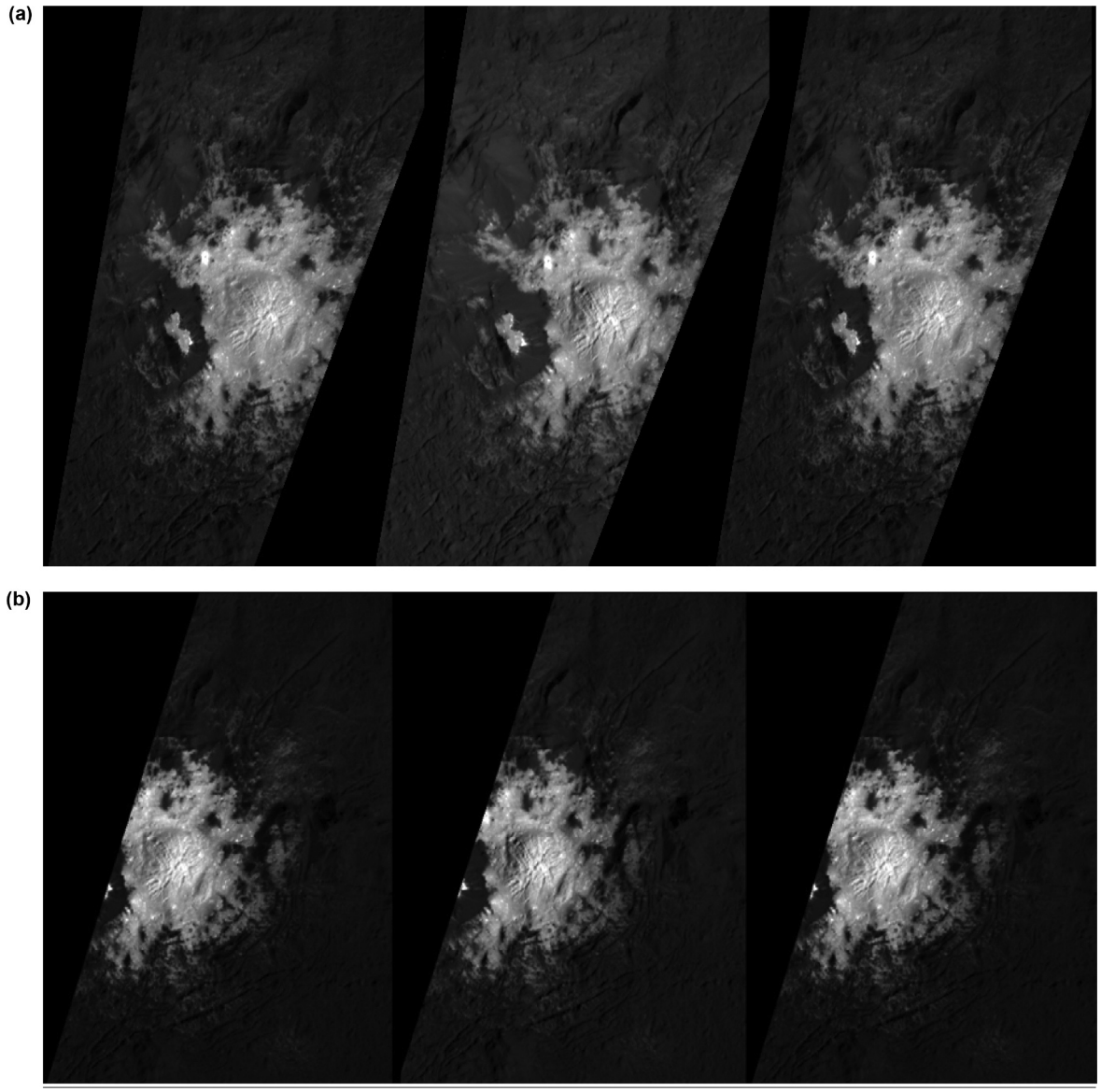

Fig. 9. (a) Stereo anaglyph of central pit and domes structures in Occator crater, Ceres. Images were acquired at pixel scales of ~35 m. Note deep pit to upper right just beyond edge of bright deposit that is not covered or filled by it. View is contrast stretched to emphasize the brighter pit floor; north is to upper right. Figure format allows user to view in either wall-eyed model (left-center) or cross-eyed mode (center-right). (b) Stereo anaglyph of central pit and domes structures in Occator crater, Ceres, centered on the eastern massif. Images were acquired at pixel scales of ~35 m. View is contrast stretched to emphasize the brighter pit floor; north is to upper right. Figure format allows user to view in either wall-eyed model (left-center) or cross-eyed mode (center-right).

sub-km-wide bright spots at their center (Fig. 13). Why some bright deposits should form near the major east-west trending fractures but not others is not understood.

The bright material in many of these patches are concentrated in the lows between the knobs and ridges that make up lobate floor material, or are brighter on the side of the ridges facing the center of each patch (Fig. 13). These patterns suggest we are locally seeing small-scale topographic control of bright materials that could have been deposited ballistically in a radial fire-fountain style or explosively from a central area (e.g., Zolotov, 2017; Ruesch et al., 2018, this issue; Quick et al., 2018, this issue; and Nathues et al., 2018, this issue), or downslope accumulation of such material in lows.

Several crater-like pits <1 km across with dark floors and haloes are also interspersed with and superposed on bright material in the Vinalia Faculae complex (Fig. 13), especially in the eastern most sections. They could be small impact craters that excavated dark material from below.

Together, these observations point to topographic control of bright spot formation (or preservation) on local scales, at least in part. The sinuous traces of bright material in the central depression (Figs. 8, 9 and 11) are slope controlled, while isolated mounds form partly covered higher standing dark spots or “islands” within the bright deposit. The flat-lying lobate floor-fill units typically have a sinuous, knobby, or ropy texture (Fig. 7), and we postulate that with the bright patches of Vinalia Faculae (Fig. 13) we are also seeing small-scale topographic control of bright spot materials, with material filling local lows and high-standing knobby material forming darker ‘islands’ within the bright deposits. In some areas, however, bright material appears to form on top of or on the sides of local highs, indicating that some bright material may be deposited directionally, possibly implicating ballistic air fall. Downslope mixing of dark and bright material complicates interpretation. Several emplacement processes may be in play, including ballistic air fall, extrusion of materials from multiple point or fissure sources, and downslope migration to local lows, including closed basins with no inlet or outlet. The variability in inferred morphologies suggests, however, that we may be near the resolution limit of resolving bright material emplacement mechanisms in the 35 m/pixel imagery.

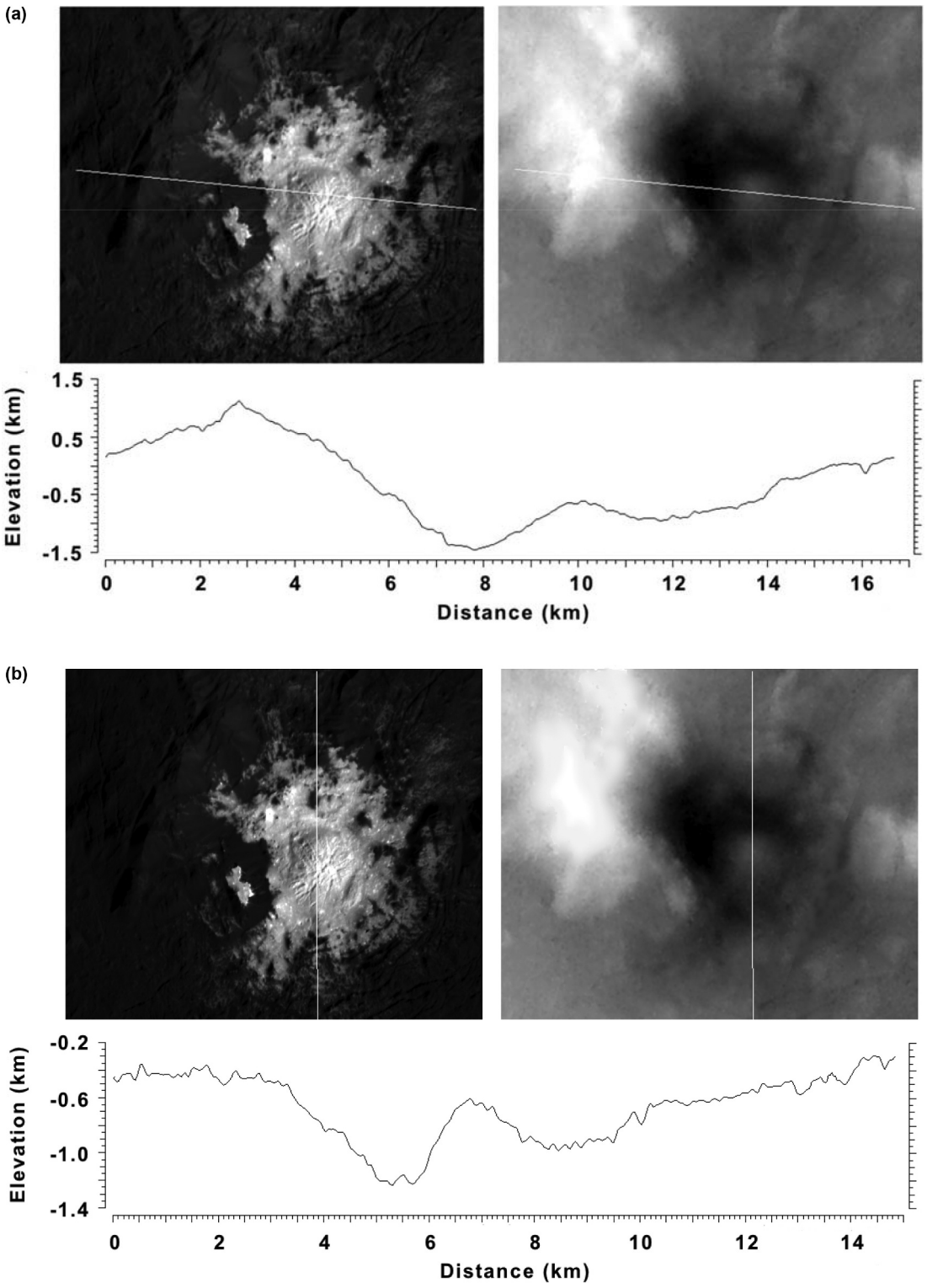

Fig. 10. Image (left), DEM (right), and topographic profile (bottom) across central structure of Occator crater, Ceres, showing central pit, central dome and flanking massifs. Left is Framing Camera mosaic, right is DEM from stereo images. Width of scene is 18 km; north is up. View shows western massif along rim of central pit and central dome in Occator crater. Lines show location of profiles.

3. Occator Crater central structure in context

3.1. Central pits on Ceres

Large craters in the 40–150 km size range are numerous across Ceres, and while none are as well preserved as Occator, they do provide an important basis of study. Our catalog of well-preserved crater morphologies on Ceres reveals that ~11 out of 14 craters between 75 and 150 km across whose central structures were not obscured by post-impact modification (usually smaller cratering events) possess partially rimmed central depressions or pits (Fig. 14; Schenk et al., 2016). Craters between ~50 and 70 km often have disrupted or disorganized central peaks, suggesting that incipient pit formation may be initiating at smaller diameters. We therefore conclude that pit formation is the

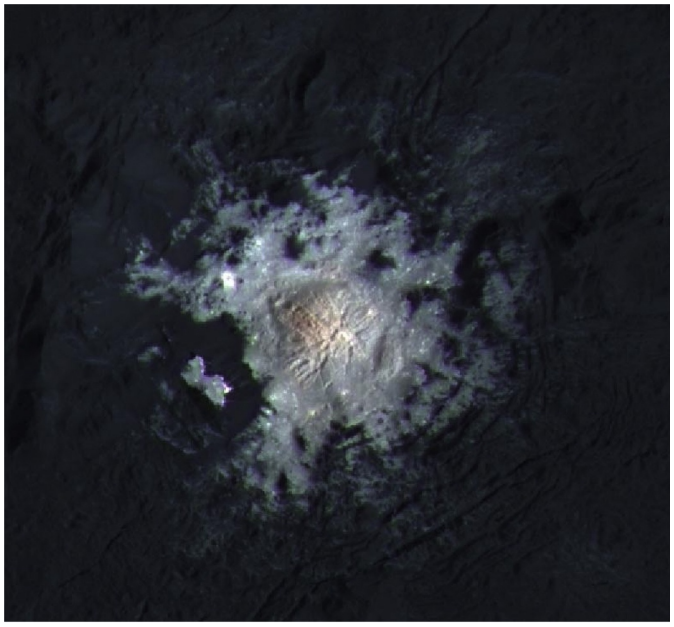

Fig. 11. Three-color view of the Occator central dome. Images acquired at 35 m pixel scales; north is up. Scene width is 20 km. Filters used are 965, 555 and 438 nanometers.

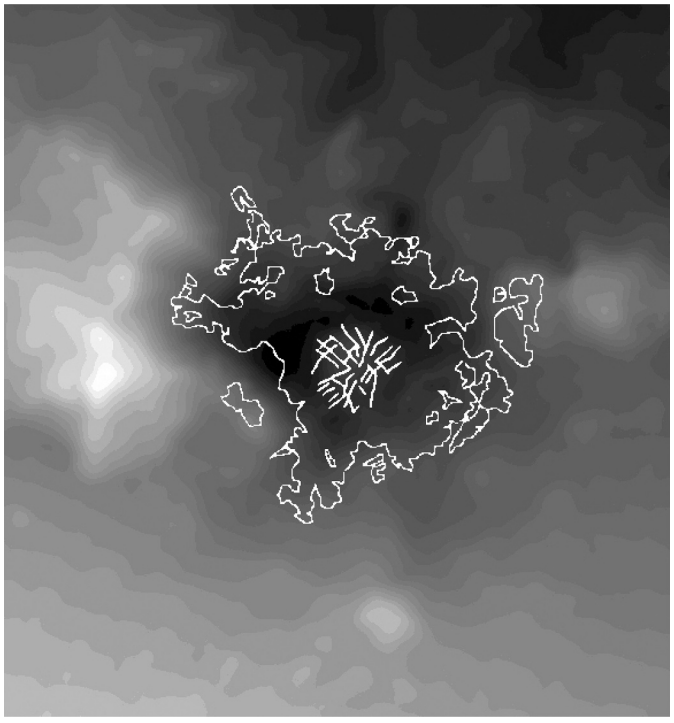

Fig. 12. Closeup of Occator region DEM (from Fig. 1) showing central pit and dome. Highlighted in white line is the outline of the bright carbonate deposit Cerealia Facula, showing relationship to topography. Also shown are the most prominent fractures on the central dome (bright crossed lines at center). Total topographic range depicted is 3 km.

dominant process in the 75–150 km size range on Ceres and is diagnostic of crater processes in the outer shell of Ceres.

Central pits on Ceres exhibit a range of morphologies comparable to those observed on other bodies. While noting that Occator is among the best preserved of these large craters on Ceres, several illuminating comparisons can be made. In each of the observed central pits (e.g., Fig. 14), the pit rim is asymmetric and usually incomplete, with angular massifs or amphitheater enclosures common along the raised rim. The central pits of Toharu (Figs. 14–16) and Chaminuka (Fig. 14) are illustrative in that their pit rims ramp up in elevation from the crater floors and have pit floors elevated above the crater floor, only to crest in a large amphitheater shape depression. This suggests that an otherwise normal peak would have formed except that its crest did not form or was removed. In these craters, the raised pit rims are mostly or nearly complete in circumference. These are referred to as peak-pits or summit pits (e.g., Barlow et al., 2017). The pit floor at Toharu appears to form and extended lobate deposit outward and downslope onto the crater floor (Fig. 16), suggesting the possibility that the top of the central peak partially collapsed as incoherent debris and slid onto the floor. These high-relief pit rims are also located at latitudes of 48° to 58°, and contrast with those at more equatorial latitudes which usually have low relief or missing pit rim walls (e.g., Nawish, Dantu, Occator and Gaue), suggesting a latitudinal dependence on the coherency of central peaks and pits on Ceres.

At the other extreme, the pits of some craters such as Gaue and Nawish (Fig. 14) exhibit pits with floors depressed below the crater floor and with little or no massifs or rim constructs. These are sometimes referred to floor-pits. Other craters, including Occator, have morphologies intermediate between summit- and floor-pits. These craters have raised pit rim massifs but only around a portion (circa $<$ 50%) of their circumference. These can be referred to as partial rim pits. In a sense, these designations are merely an expression of what is likely to be a continuum of structural expressions of the observed central uplifts in Cerean or icy body craters.

None of the other central pit craters observed on Ceres (e.g., Fig. 14) feature a central dome similar to that observed at Occator. While the floor of the Dantu pit features a number of low hummocks (Fig. 15), they are somewhat degraded and their origins are cryptic. All the other pit craters show considerably more landform degradation than does Occator. Whether the lack of additional domes on Ceres is due to fragility of the fractured dome, leading to slope failure or collapse, burial due to erosion or partial collapse of surrounding pit rims, or a failure to form other domes in the first place is not obvious from current data.

3.3. Central pits on Mars

Central pit craters have been observed on Mars (e.g., Barlow et al., 2017, and references therein). While it is beyond the scope of this project to survey Martian pit craters in detail, as this has been done elsewhere, there are broad similarities and differences with those observed on Ceres. Mars is of particular interest as the outer layers of Mars are likely to be dominated by silicates with an admixture of interstitial water ice (e.g., Goossens et al., 2017). (The estimated density of Mars' crust of $\sim$2.5 g/cm^3 (Goossens et al., 2017) is more than twice the estimated mean density of Ceres' crust (at $\sim$1.15 g/cm^3) and Ceres is likely to have a considerably higher percentage of salts and ice (Park et al., 2016; Fu et al., 2017).) Further, surface gravity of Mars is 13 times greater than on Ceres, which will require significant gravity scaling to make effective comparisons.

Martian central pits exhibit a similar range of morphologies from summit pits to floor pits Mars (e.g., Barlow et al., 2017) that are seen in our smaller sampling on Ceres. Unlike Ganymede or Callisto, central pits do not overwhelmingly dominate their crater diameter range in the way they do in icy bodies. Possible origins and influences of water ice on Martian pits are discussed in the later sections. Barlow et al. (2017) give a median diameter of central pit craters on Mars of $\sim$16 km, well below our cerean pit crater range and consistent with a role for surface gravity on pit crater formation in mixed ice-rock targets.

A few central pit craters are observed on the Moon and Mercury (e.g., Xiao et al., 2014). These are uncommon to rare on these bodies and not considered further. One factor that must be considered in the formation of some central pits, particularly those that are small compared to the norm, is that pits may be a topographic artifact of

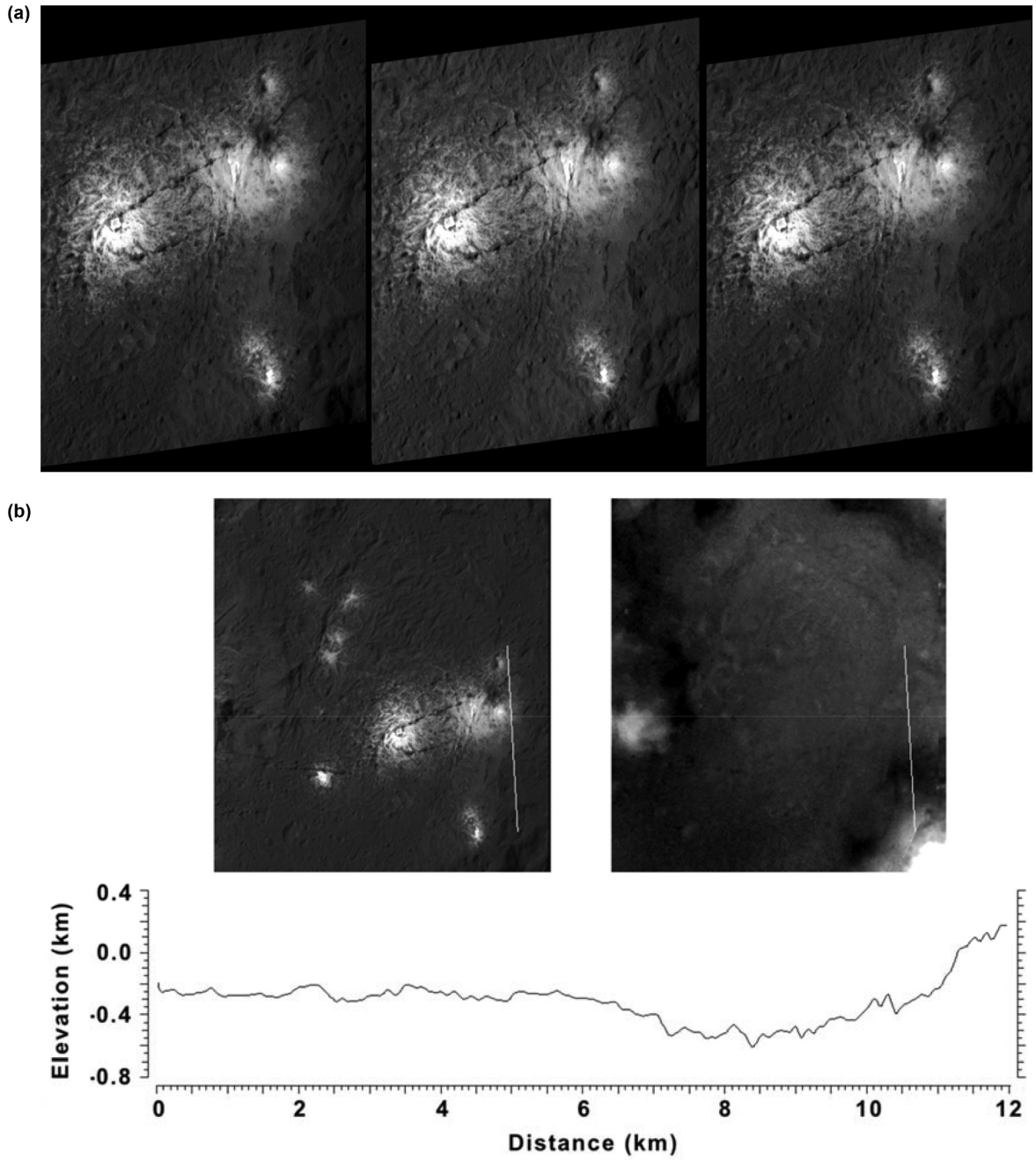

Fig. 13. (a) Stereo anaglyph of Vinalia Facula region in Occator crater. View is almost entirely on low relief lobate floor-fill deposits. Images acquired at 35 m pixel scales; north is to upper right. Figure format allows user to view in either wall-eyed model (left-center) or cross-eyed mode (center-right). (b) Image (left), DEM (right), and topographic profile (bottom) of bright deposits of Vinalia Faculae and eastern lobate floor material at Occator. The slightly elevated plateau is part of the crater floor fill. Note the lack of topographic expression in this DEM, which has a topography precision of ~100 m.

incomplete or unusually disorganized central uplift processes, which normally involve the uplift of highly folded, faulted and compressed materials. This effect would not be likely for larger central pits such as those shown in Fig. 14.

3.3. Central pits on icy satellites

Central pit craters have been known on the large ice-rich Galilean satellites Ganymede and Callisto since Voyager (e.g., Passey and Shoemaker, 1982; Schenk, 1993; Alzate and Barlow, 2011; Bray et al., 2012). Like Mars, the icy Galilean satellites are of interest for their composition. While Ganymede is strongly differentiated into an ice crust and mantle, Callisto may be of special interest in that it is likely to be only partially differentiated (e.g., Schubert et al., 2004) and its outer layers could be of mixed silicate-ice composition, perhaps analogous to what is observed on Ceres.

Galileo contributed only marginally to our global survey of these features and observed no pristine central pit craters at resolutions comparable to Dawn at Ceres (~35 m/pixel). The best Galileo pit crater observations were in the 130–180 m/pixel scales and either under high-Sun illumination or of craters that had been degraded due to age. Further, the best observations were of pit craters in the > 50 km size range. Thus our comparisons, though important, are necessarily limited.

Central pit craters are by far the dominant crater class in the > 25 km diameter size range on Ganymede and Callisto and fall into

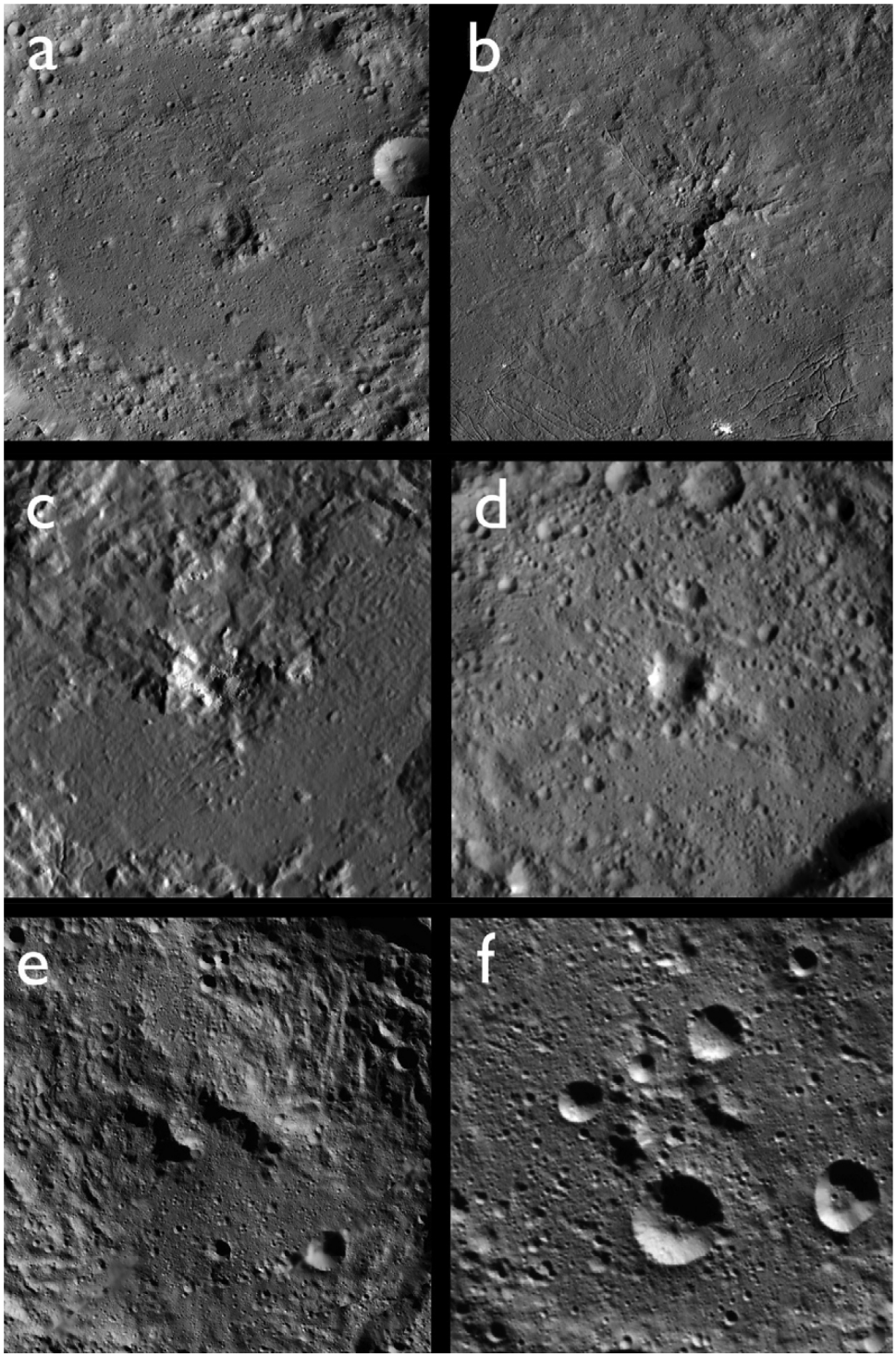

Fig. 14. Six prominent well-preserved central pit structures on Ceres. From upper left: (a) Gaue (Dc ~ 86 km; Dp ~ 8 km), (b) Dantu (Dc ~ 123 km; Dp ~ 11.5 km), (c) Occator (Dc ~ 92 m; Dp ~ 9 km), (d) Nawish (Dc ~ 77 km; Dp ~ 8.5 km), (e) Toharu (Dc ~ 87 km; Dp ~ 9.5 km), (f) Chaminuka (Dc ~ 128 km; Dp ~ 13 km). Occator map is a shaded relief rendering from the topography used in order to show relief across the central structure without the contrasting albedo patterns. Illumination is from the right in all cases.

two gradational classes (Schenk, 1993; Schenk et al., 2004): central pit and central dome craters. The former are those in which the small central peaks observed in smaller craters are replaced by central depressions of similar relative size with irregular and incomplete raised rims (Fig. 17). Like Mars, many variations in pit morphology occur, from summit-pits (which are more common in smaller such craters, to floor pits with less evidence for pit rim relief and massifs. Thus, these icy central pits resemble the central structures we observe on Ceres (Fig. 17), despite the fact that Ganymede at least is a differentiated object with an outer zone likely dominated by water ice (unlike Ceres where water ice comprises no more than ~30% of the outer layers.

The central pits of Ceres and the large icy satellites are distinct from peak-ring basins on terrestrial bodies such as the Moon and Mercury in that the rims of central pits are much smaller with respect to crater diameter. The primary difference is the smaller aspect ratios of central pits. Pit-to-crater diameter ratios (Fig. 18) are ~0.1–0.2 (Schenk, 1993)

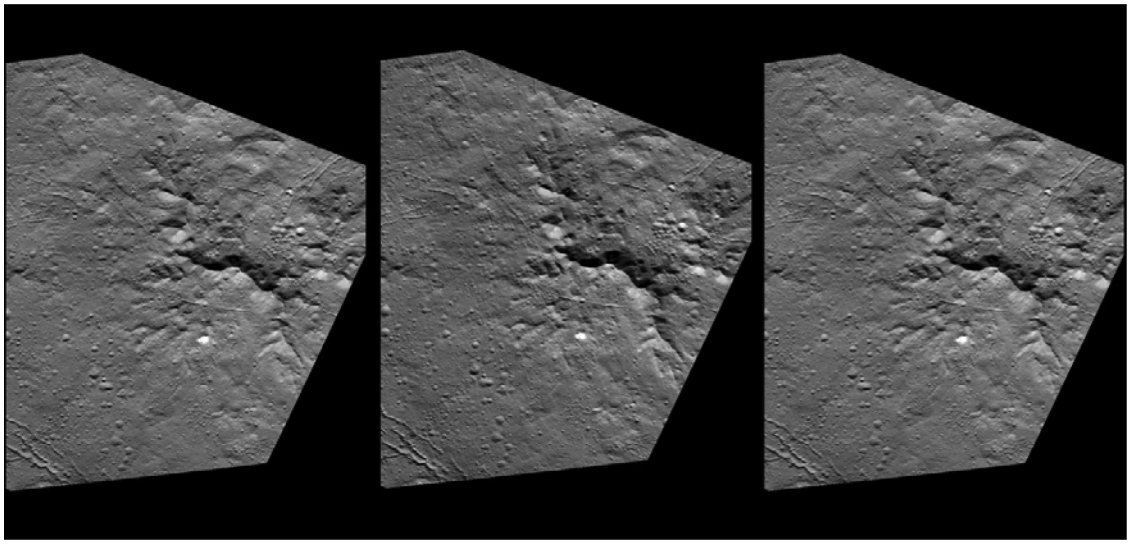

Fig. 15. Stereo anaglyph of central pit region of Dantu crater (upper right) and floor deposits. Images acquired at 35 m pixel scales; north is to upper right. Figure format allows user to view in either wall-eyed model (left-center) or cross-eyed mode (center-right).

while peak rings have ring-to-crater diameter ratios of ~0.5 (Pike, 1980). Pit rims tend to have more asymmetric morphologies, including amphitheater-like scarps to incomplete massif rings (Figs. 14–16).

Central dome craters on Ganymede and Callisto (e.g., Schenk, 1993; Schenk et al., 2004) are similar to central pit craters, except for the broad rounded dome that partly fills the central depression, flanked by the high-standing ring of knobs or massifs (Fig. 19). The transition from central pit to central dome craters occurs at ~60 km on both icy satellites. As only one central dome is known on Ceres, the transition diameter there is unknown.

While Galileo did obtain high-resolution images of several large central domes 25–40 km across at 90–180 m pixel scales, it did not obtain any of the smaller domes that are most similar to what is observed at Occator. These domes are also a few kilometers across and are evident in the <1 km-pixel-scale images that were acquired by Voyager for parts of these surfaces (Fig. 19). While it is not possible to determine whether these smaller domes are also fractured, we conjecture that the next high resolution images obtained of either satellite will reveal fractures similar to those on Ceres and larger domes on Ganymede and Callisto.

Galileo images of the large central domes at Doh (Callisto) and Neith and Melkart (Ganymede) all show extensive fracturing across the tops of these domes (Fig. 20). The processes fracturing the Occator dome and those on Ganymede and Callisto may be both common and fundamental characteristics of craters in these size ranges. Fracture style may be related to dome morphology, but as we cannot resolve fractures on similar-sized domes on Ganymede or Callisto, nothing can be said at present about any similarity in style or composition in the two planetary systems.

Resolved topography of central domes is available for only 5 craters on Ganymede and Callisto, and all larger than ~25 km across. The Ganymede/Callisto examples indicate mean heights of 1 to 1.5 km, with a possible increasing trend in height with crater and dome diameter (Fig. 21). The measured height-to-width ratio of the Occator dome is ~0.25, ~10 times greater than Ganymede domes, but the Occator dome is also a factor of 10 smaller across than any of the Ganymede domes for which we have high-resolution data. Without additional examples on either body it is not possible to determine whether or not there is a threshold height of ~1 km for smaller domes (perhaps related to yield strength of the materials if Ganymede domes are icy and Ceres dome ice-rock mixtures) or whether the lower gravity on Ceres allows domes to maintain a greater height than on Ganymede. Once again, however, we are handicapped by the less robust knowledge of dome composition and stratigraphy on those icy satellites.

Extrapolation of the observed transition diameter to central pits on Ganymede and Callisto [based on inverse gravity scaling of simple-to-complex transitions generally (e.g., Pike, 1980; Schenk et al., 2004); see below], predicts that for similar target compositions and conditions central pits will occur in craters larger than ~60–90 km for the Saturnian satellites and Ceres (Fig. 22). We have not described central pit craters on the midsize icy satellites of Saturn, Uranus and Pluto (i.e., Charon) because with one exception [Odysseus on Tethys (Barlow et al., 2017; Schenk et al., 2018)] they do not exist even in impact basins as large as 450 km-across (e.g., Schenk, 1989). The Odysseus central complex is essentially an annular ring of low rugged massifs ~120 km in diameter surrounding a circular depression ~60 km wide and ~4 km deep with respect to the basin floor. With the exception of Odysseus, the 12 or so central "pit" craters identified by Barlow et al. (2017) on Saturn's icy moons, are not classical pit craters but erosional or degradational features and are statistically overwhelmed by the 1000's of central peak craters that are not at all pit-like.

4. Origins of central pits and domes

Dawn mapping of Occator crater reveals a relatively young well-preserved impact crater on Ceres dominated by extensive lobate floor deposits and a complex central structure (Figs. 1 and 2). A wealth of topographic and surface detail is revealed, some of which are familiar from other planetary objects, some of which are unique to Occator and Ceres and probably reflect the unusual (crustal) composition of that body. Based on Dawn gravity studies (Konopliv et al., 2018; Ermakov et al., submitted; Mitri et al., submitted), the density of Ceres' outer layers is ~1.2–1.3 g/cm3; silicates represent a minor fraction of the crustal material, less than 20 wt.%, and hydrated salts <18 vol.% (based on cosmochemical abundances, Castillo-Rogez et al., submitted), with clathrate hydrates the more likely explanation for the high strength of the crust, and water ice making up the rest. Because Ceres' crustal layers contain some water ice, the ice-rich satellites of Jupiter and Saturn are useful constraints on observed complex crater morphologies on Ceres, including central pits and domes.

4.1. Origin(s) of central pits on ceres

The discovery that partially walled central depressions (i.e., pits) are the dominant landform in larger craters on Ceres between ~70 and

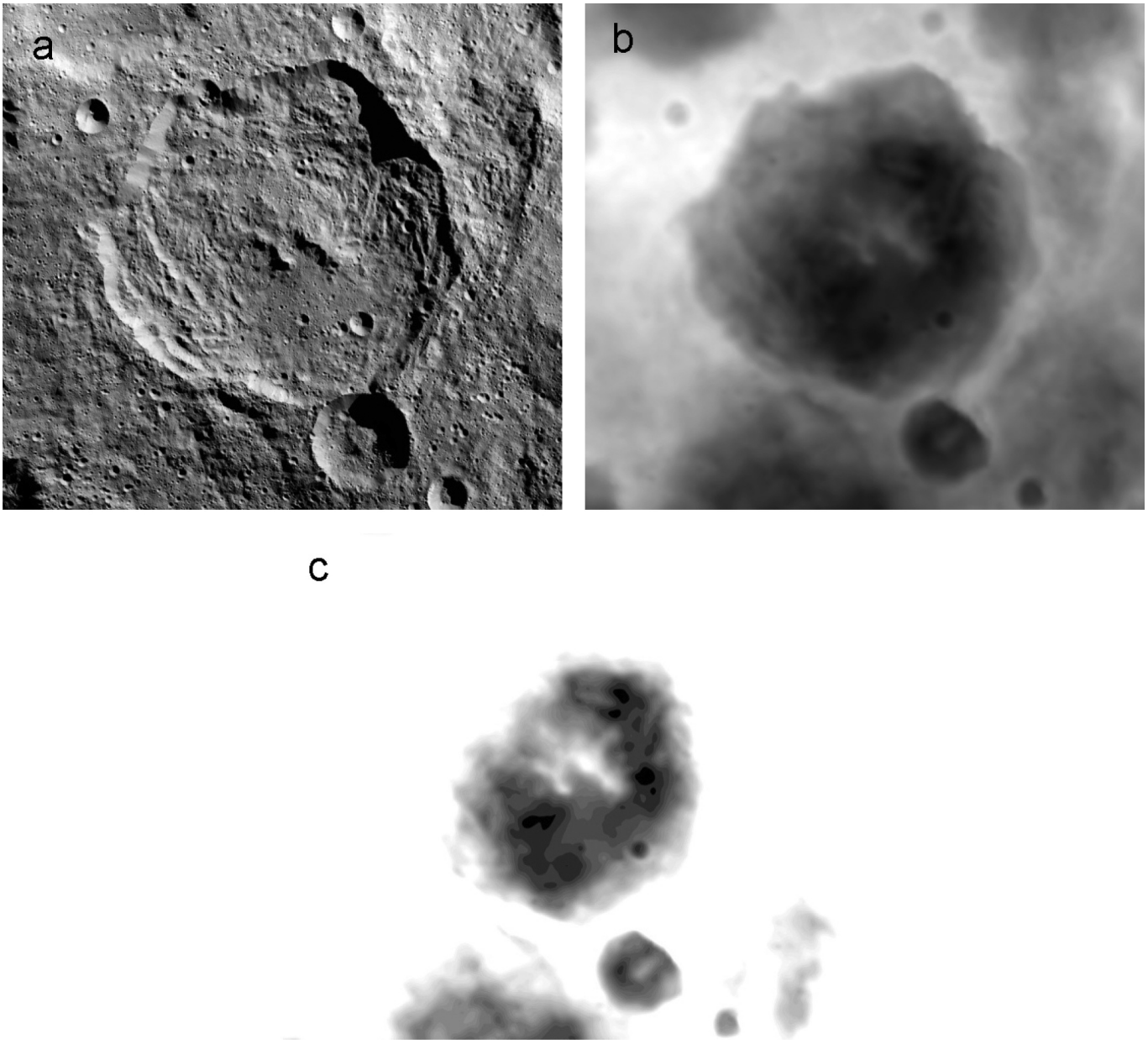

Fig. 16. (a-c). a) Image mosaic of Toharu crater (D = 87 km). b) DEM of Toharu crater. c) DEM of Toharu, scaled to highlight the floor and central peak-pit region, and deposit extending south from central pit.

150 km was something of a surprise (Schenk et al., 2016), primarily because of the absence of such structures on any of the icy Saturnian satellites (e.g., Schenk et al., 1989), key ice-rich objects similar in size and density to Ceres. The inference was that central pits, while the primary morphology in craters on Ganymede and Callisto between ~30 and 60 km diameter (Schenk, 1993), could not form on lower gravity bodies. Central pits also occur sporadically in many martian craters (e.g., Barlow et al., 2017 and references therein) and even a few lunar craters (e.g., Xiao and Komatsu, 2013), but are not dominant and hence may represent variations in target conditions or processes unique to Mars rather than a diagnostic impact process.

Can central pits on Ganymede and Callisto be compared with those observed on Ceres, given the differences in thermal and compositional properties of the two target types? Aside from the fact that they are the only other commonly observed examples of this morphology in the Solar System, central pit on Ganymede & Callisto have rather similar morphologies to those on Ceres (Figs. 17 and 18), including incomplete knobby or partially rimmed morphologies of the pit rim (Figs. 17 and 19) and similar D_{pit}/D_{rim} ratios (Fig. 18). Even the single known central dome on Ceres has a similar rounded fractured morphology to the pit domes on Ganymede and Callisto (Fig. 20). These comparisons suggest that the physical processes of pit formation on the three bodies may bear some similarities and warrant comparisons. It is interesting that Callisto might also have a significantly larger percentage of non-icy materials within its crustal layers (e.g., Schubert et al., 2004) and yet craters are to first order indistinguishable from those on differentiated Ganymede (e.g., Schenk, 1993; Schenk et al., 2004).

On Ceres, most craters between ~70 and 150 km have central pits instead of central peaks (craters between ~50 and 70 km often have disrupted or distorted central peaks, suggesting that incipient pit formation may be initiating at smaller diameters). There are several older large craters where the central region is obliterated by post-formation impact events, and hence the number of known central pit craters on Ceres is limited to ~11. We therefore conclude that pit formation is the dominant process in the 70–150 km size range on Ceres and is diagnostic of crater processes in the outer shell of Ceres.

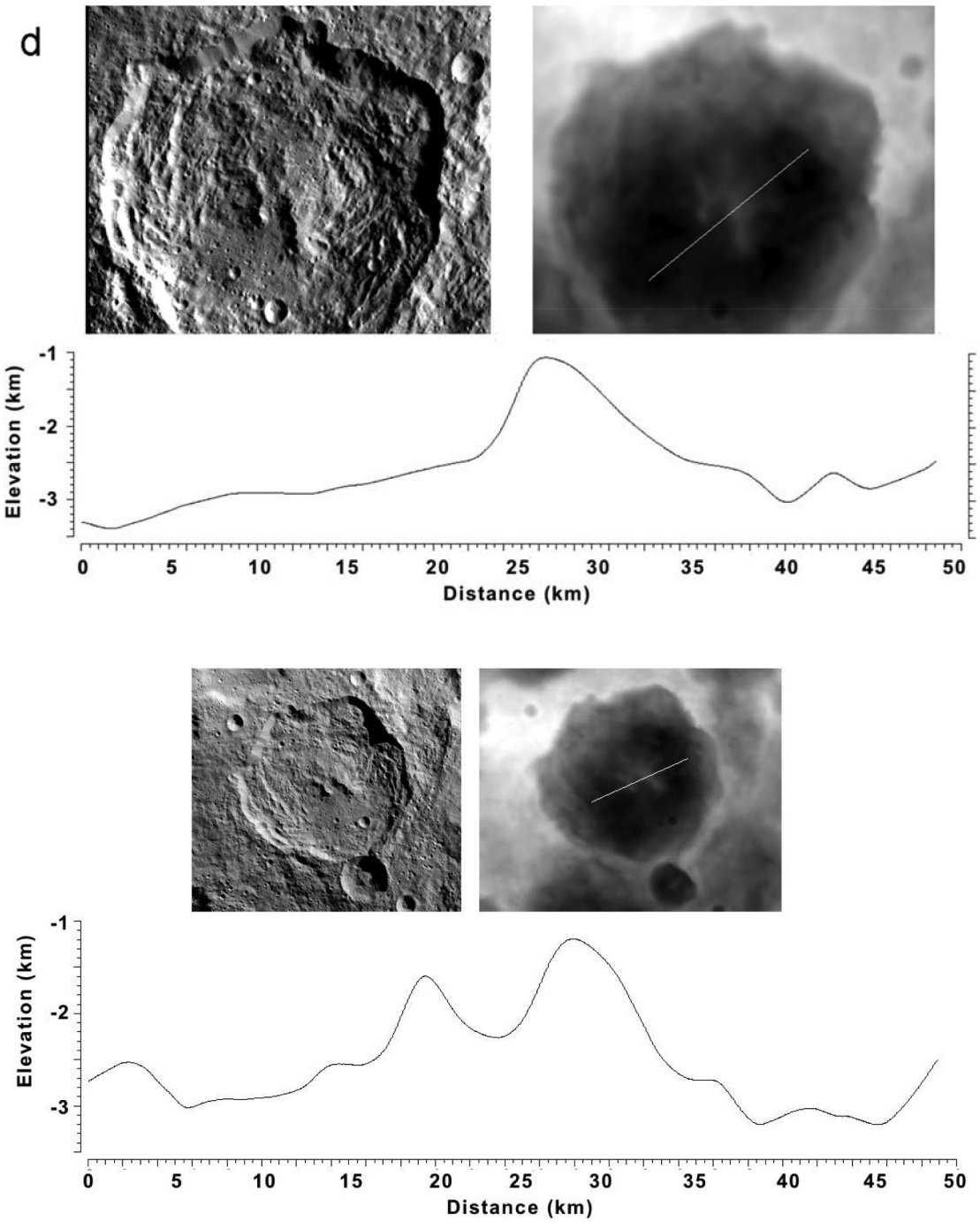

Fig. 16. (d) Profiles across Toharu central pit and lobate deposit, and central pit, showing elevation above crater floor.

Unlike other morphologic transitions (Fig. 22), the peak-to-pit transitions observed on Ganymede and Callisto do not scale inversely with gravity to the smaller icy satellites of Saturn and Uranus. In fact, the peak-to-pit transitions on Saturnian icy moons must be > 350 km for all these moons as the largest craters observed there are of this size and only 450 km Odysseus and perhaps 135 km Ursula on Titania have a pit-like central morphology (Schenk, 1989; Schenk et al., 2018).

In contrast to the missing central pits on Saturn's moons, the peak-to-pit transition on Ceres at 65–75 km is quite consistent with inverse-gravity scaling from Ganymede/Callisto (Fig. 22). That Ceres follows this trend while Saturn's moons do not suggest that the Saturnian moons are anomalous, and provides a key constraint to the origin of central pits generally. The consistency of other morphologic transitions on Ceres with those of the midsize icy satellites (Fig. 22; Schenk et al., 2016) indicates that cratering transitions on Ceres including central pits are dominated by the weakest components, i.e., the ice phases. This is likely due to ice controlling the rheologic response of the crust *during* the high-strain-rate impact event, and is the only way to explain the inferred low-ice content (< 30%) inferred from gravity and shape (Fu et al., 2017), and the stiffening of the crust at low strain rates evidenced by the lack of viscous relaxation (Bland et al., 2016). Impact velocities on the target bodies in question are all 5 km/s or higher. The most obvious difference then is that the Saturnian moons have significantly colder surface and internal temperatures than Ceres or (to a lesser degree) Ganymede or Callisto, which may inhibit the mechanism of pit formation, whatever that may be. We conjecture that colder

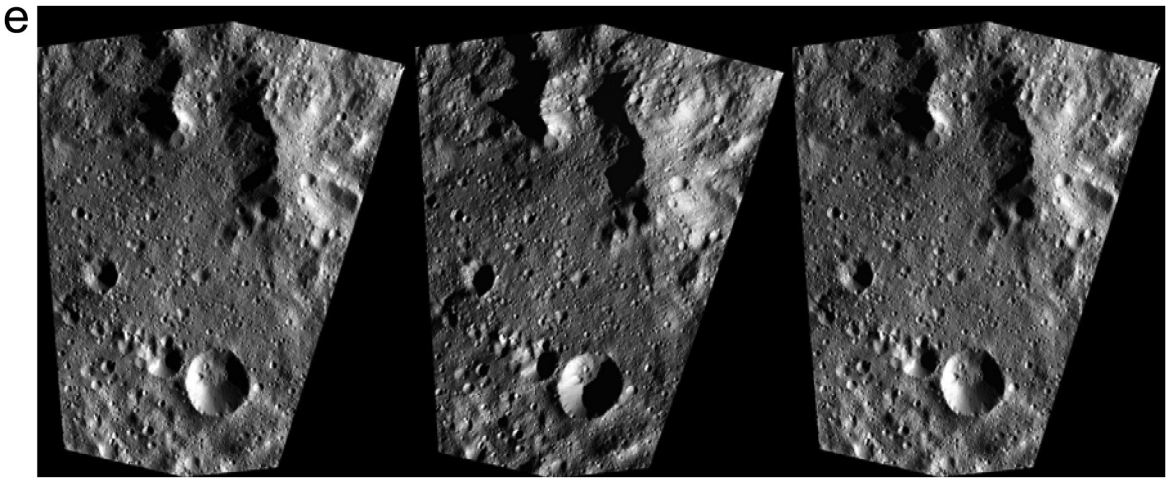

Fig. 16. (e) Stereo anaglyph of central region of Toharu crater. Rimmed central pit is at center top. Images acquired at 35 m pixel scales; north is to upper right. Shifting Sun elevation causes some shadow differences. Figure format allows user to view in either wall-eyed model (left-center) or cross-eyed mode (center-right).

temperatures may also preserve a greater degree of porosity on the midsize icy moons than on Ceres.

A possible indicator supporting the potential influence of temperature on central pit formation is the lack of any central pit craters on Ceres poleward of ~60° latitude. The only two examples of craters larger than 75 km across where we can identify the central structure and that have classical conical central peaks on Ceres are at these higher latitudes (Zadeni, D ~ 124 km (Fig. 23) and the 85 km-wide crater at 62°, 237°E). Further, there is the tendency for pit rims at equatorial latitudes to have less relief and less 'completeness' than those at mid-latitudes of 45–60° (Fig. 14). We also note that the lobate and smooth floor deposits observed at most craters on Ceres > 40 km across (Schenk et al., in 2016) are also absent in Zadeni and other large polar craters, indicating that extensive impact melting did not occur there. While the total number of large craters poleward of 45° is limited and not statistically overwhelming, both observations are consistent with a progressive equatorward degradation or loss of central peak materials. Polar temperatures on Ceres are tens of degrees colder than in more equatorial latitudes (e.g. Bland et al., 2016; Hayne and Aharonson, 2015), and this could exert a similar control over pit and lobate/smooth floor material formation as the colder conditions may do on Saturn's icy moons.

There is as yet no consensus as to the origin of central pits and why they replace central peaks and in larger craters. At least four models have been proposed to date but each has difficulty explaining all observed features. A particular problem has been that Galileo acquired no imagery of well-preserved pit craters at resolutions better 150–200 m pixel scale, rendering testing of models difficult.

The first model is the explosion pit model (e.g., Wood et al., 1978), where accumulated subsurface vapors or gases subsequently explode violently. While potentially valid for some martian craters (Williams et al., 2014), no evidence has been found to support an explosive event at these pits on Ganymede, Callisto or at Occator, as no large piles of debris are evident either in the pits or scattered around them. Williams et al. (2014) suggest that coarse-grained material evident in thermal inertia data surrounds central pit craters on Mars and that this is evidence of an explosive event at the central pit. They do not make the test of examining central peak craters to determine if similar deposits are there as well, which would suggest that they are related to the uplift process generically and not pit formation.

The second model is the layered target (Greeley et al., 1982) or ductile intrusive model (Moore and Malin, 1988; Schenk, 1993), in which impact occurs in a rheologically layered target and the impact excavation and collapse processes are sensitive to these differences. Ductile material is uplifted through and displaces a more brittle surface layer after or during the crater event as part of the central peak, forming the rounded dome and rugged pit rim we see today. Like the others, this model was not adequately tested by Galileo observations, and remains on the table. The inferred sequence of dome formation after pit and bright deposit formation at Occator, however, would appear to rule out a prompt dome formation for Ceres at least.

The third model is the collapse of a central peak comprised of structurally or compositionally weak material, which would fail laterally (e.g., Melosh et al., 1982; Croft, 1983). While the dimensions of the central pit and its elevated rim are consistent with the possible presence of a former but now partly lost central peak, there is a serious problem with volume, as a mountain cannot produce a depression through simple collapse. Nor is the volume of remaining uplifted material enough to explain the displaced mass. Collapse may have been part of vertical oscillations in the central uplift. This might not satisfy the morphologic constraints, as there is little evidence for an outward movement of material. Rather the central complex appears to be simply missing from an original central peak.

The fourth model is the molten plug model (e.g., Croft, 1981; Senft and Stewart, 2011; Bray et al., 2012) in which the central uplift is composed at least in part of liquid water, rather than simply uplifted ice. When uplifted through the regular collapse process, this liquid then drains away into fractures formed in the crater floor, instead of forming an intact peak. The pit rim is then the contact between the remaining solid uplifted material and the now lost liquid component. There is considerable uncertainty as to the physical reality of these models due to potential ambiguities in the numerical codes at the radial center of the crater, which often produce unrealistic spurious effects at the center. Nonetheless, this model might work for icy satellites but on Ceres, where the crust is likely to be no more than 30% ice, the uplifted plug would have to be of mixed water-rock composition. If there are clathrates, then the molten material would be mostly water with a small fraction of salts and clays and significant dissolved gas, which would assist buoyant rise and prompt fountaining at the surface. Collapse of this partially molten plug could explain the pits, especially as some of the pits have remnant flanking rims several hundred meters high that suggest a missing peak (Fig. 16).

The upward slopes and hummocky morphology at larger pits on Ceres (Fig. 14) and the two large massifs adjacent to the central pit at Occator (Figs. 8 and 9) are consistent with the notion that pits are remnants of or partially formed sections of a missing central peak. The apparent preservation of larger pit rim segments at higher latitudes and the possible lack of central pits at all at polar latitudes also imply temperature and therefore melting are at least involved in pit formation on Ceres.

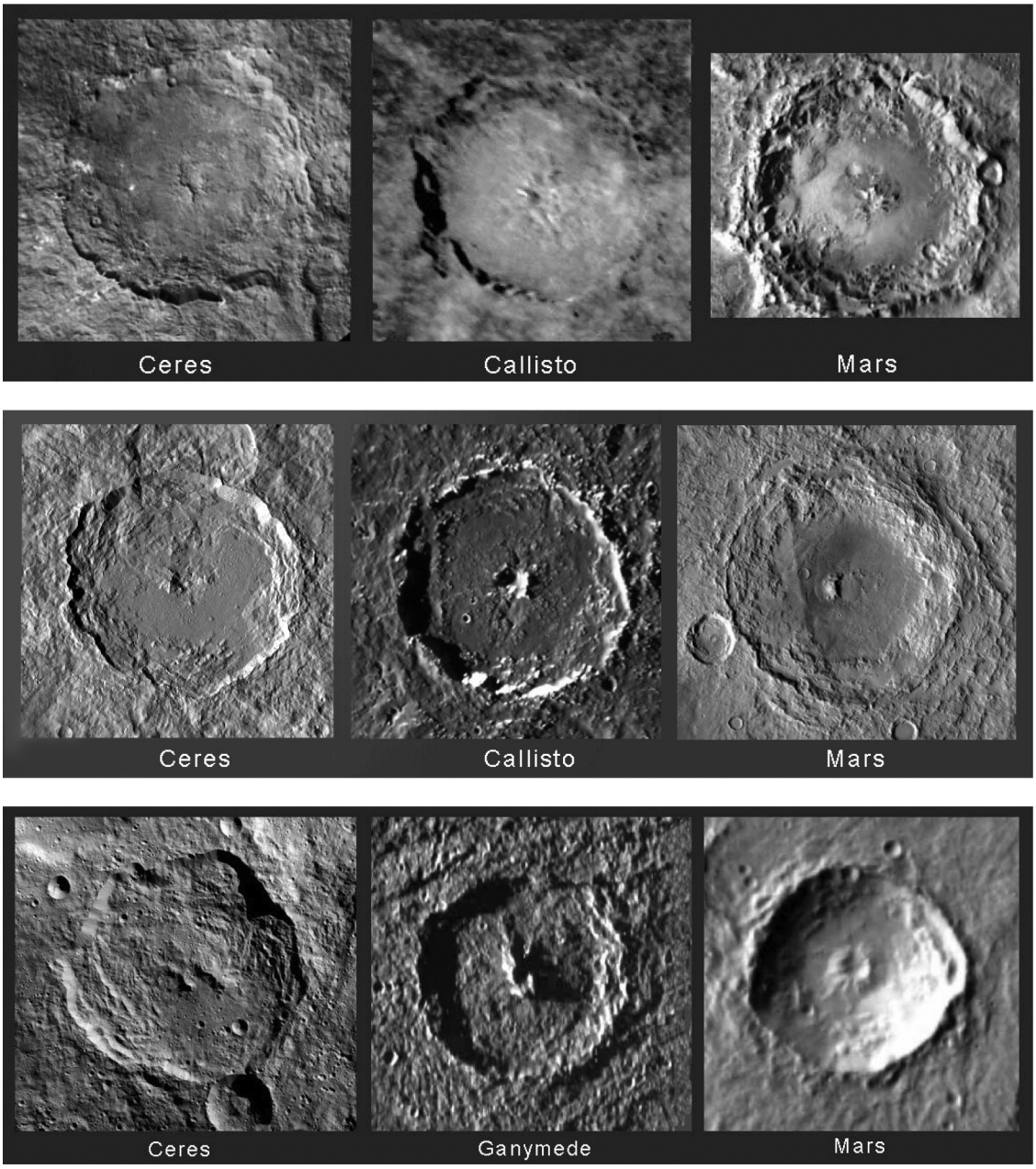

Fig. 17. Three sets of images comparing central pit craters on Ceres (left) and Ganymede and Callisto (center), and Mars. Top row: floor-pits, displaying little or no flanking rim topography (left-to-right: Dantu [125 km] unnamed Callisto crater [~35 km], and Cerulli crater, Mars [122 km]). Middle row: floor-pit craters showing incomplete pit rim topography (left-to-right: Occator crater in shaded relief to remove albedo variations [92 km], unnamed Callisto crater [~45 km], Hargraves crater, Mars [68 km]). Bottom row: peak-pit craters showing considerable pit rim relief (left-to-right: Toharu [87 km], Gula crater, Ganymede [40 km], and unnamed Mars crater [45 km]. The comparison of craters of different sizes is based on inverse scaling of crater transition diameters (Pike, 1980; Schenk et al., 2004).

That central pit rims on Ceres (and possibly Mars, Ganymede and Callisto) are remnants of central peaks is supported by comparison of pit measurements with 'intact' central peaks on Ceres. A sampling of typical central peak dimensions shows they increase linearly in height and width with diameter (Fig. 24). To compare to central peak widths, the total observed lateral extent of the well preserved pit rim massifs at Toharu (Figs. 14 and 16) is ~25 km wide and ~2 km at its highest, both similar to values expected of a central peak in a crater of this size (Fig. 24). Similarly, the lateral extent of the western and eastern massifs at Occator, the only preserved segments of the pit rim complex there, would give a total width ~30 km, again similar to central peaks. Thus, the sloping outer flanks of central pits on Ceres (e.g., Fig. 14), to the extent they are preserved, are consistent with partial preservation of remnant central peaks. The central pit rim complexes at some craters (e.g., Nawish, Dantu and Gaue, Figs. 14 and 15) are smaller than the trend in Fig. 24, but lobate and smooth floor fill deposits in such craters likely partly bury the bases of such edifices. While the maximum height of the western massif at Occator relative to the floor is only ~1 km, it suggests that any original peak would have been ~2 km in height.

The Toharu pit summit is ~1.6 km above the mean floor, less than the expected ~2.6 km (Fig. 22). The pit depth relative to pit rim at Toharu is ~0.8 km, giving a total height of 'missing' peak mass of ~1.8 km, and for a pit width of ~9 km, this gives a 'missing' volume of ~40 km^3. The approximate area of the apparent debris fan at the base of the pit opening to the south is ~60 km^2, indicating a reasonable mean thickness of the deposit of ~125 m, though it could be locally thicker.

While the observations seem to (weakly) favor the melted peak

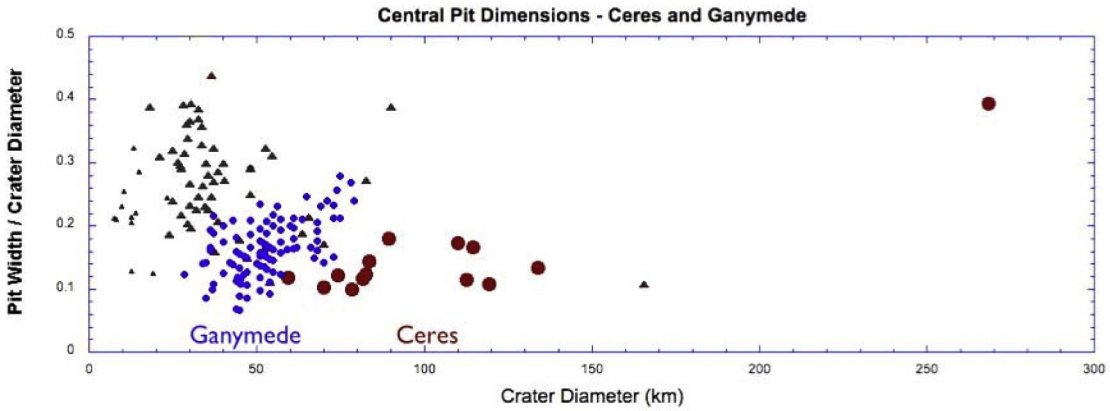

Fig. 18. Pit-to-crater rim diameter ratios for central pits and on Ganymede (small dots) and Ceres (large dots). The triangles are widths of central peaks on Ganymede. Ganymede data are from Schenk (1991, 1993). The largest value is for the central topographic ring at Yalode crater, which suggests that a different process is occurring in the largest craters on Ceres.

model at present, no one model for Occator or central pits generally satisfies all the available constraints. Basic problems in understanding central pits on icy satellites are that observational constraints are limited until we return to the Jupiter satellites system, and that numerical models historically do a poor job of reproducing small-scale structures (such as terraces, pits, fractures) in impact craters. While modeling techniques improve yearly, additional improvements are required before we can faithfully reproduce such features with confidence. Regardless of the origins, the central zones of complex craters always expose deep-rooted materials that were originally several kilometers deep (Engelhardt et al., 1992; Milton et al., 1972; Bowling et al., 2018 this issue). This must be kept in mind when examining bright materials and their origins.

A key problem in any of these models is the persistence of a depression at all through the crater collapse process. Simple collapse of a proto central peak should in principle choke the central area with debris, which is not seen except perhaps at Toharu (Fig. 16). In the melted peak model, greater degrees of impact heating will produce a deeper/thicker melted plug in the center. As described above, pit-rim complexes on Ceres are similar in size to central peaks but seem to have had most of the original core of the peak material removed. The missing transient molten peak material could have flowed into the fractured crater floor and been absorbed into the subsurface. If so, tens of cubic kilometers of material are missing from the observed crater. Yet it remains to be demonstrated that this process will in fact remove sufficiently large quantities of material to effectively make central peaks disappear. It seems unclear that such a large volume of void space could exist to absorb this missing mass beneath any crater. Are the fracture systems beneath impact craters in fact permeable and are large volumes of pore space available to be filled beneath crater center, as proposed by Elder et al. (2012)? Do minerals precipitate along fracture walls, closing them off to further drainage? Certainly fractures in the centers of terrestrial craters are filled by mineral deposits indicative of mineral precipitation (e.g., Arp et al., 2013). Could the liquefied material slosh off the rising peak and onto the floor during the uplift stage? This could lead to flow textures on the outer flanks of the central pit that might be evident as scoured textures in a few cases (Fig. 14).

We must still conjecture what a melted central peak at Occator would have been made of and how it would have behaved. We explore two possible answers to these questions. Mapping of terrestrial impact craters shows that uplifted central peaks are coherent though highly folded and fractured basement rocks uplifted from several kilometers depths (e.g., Milton et al., 1972; Wilshire et al., 1972; Kenkmann, 2002). If the impact process is similar on Ceres, then water ice might be expected to be finely distributed throughout disrupted uplifted central peak material. Impact models for Ceres (Bowling et al., 2018 this issue) indicate temperatures within the uplifted central peak will be above the melting point of water ice and thus this component will be distributed as pockets and pores of liquid, undermining the strength of the uplifted material. While the water can be expected to drain away through the dense fractures throughout the uplifted peak, we still have a volume problem regarding the remaining non-water components: where did it go? At Toharu there is the suggestion of a debris deposit flowing downhill from the pit onto the floor (Figs. 14 and 16), but this is unusual. We have a topographic depression instead of a central peak at Occator and no evidence of large debris piles from the residual non-water material, either within the pit or external to it. Could the weakened material have been launched ballistically into deep space instead of being retained as part of an otherwise normal central peak?

Alternatively, there could be an unspecified segregation process that concentrates water and ice in the uplifted central peak (e.g. Elder et al., 2012). This would perhaps mitigate the missing mass problem, as a central peak mostly of water would begin to collapse and drain away into the subsurface even as it was being uplifted. It remains for models to demonstrate how melt drainage could remove a central peak within Ceres' mixed composition crustal zones. If correct, a melted central peak origin of the central pits would require the presence of significant water ice in the outer layers on Ceres.

4.2. Origin(s) of the central dome

The central dome in Occator is likely linked to the formation of the central depression in which it sits and/or to the bright material that covers it. The formation of the dome near the center of the pit indicates that the depression, which was likely highly fractured during impact to some depth, provided either a conduit for or sat over a reservoir of material that produced updoming. No other central pits on Ceres have central domes (Schenk et al., 2018), even in craters larger than Occator such as Dantu (D ~ 125 km; Fig 15). The other examples of central pits craters on Ceres are all older than Occator, however. Perhaps Occator is unique on Ceres in the formation of a central dome due to factors such as impact velocity or unusual (and unknown) regional target properties. Alternatively, domes may form elsewhere in large central pits on Ceres but are 'fragile,' as suggested by the intense fracturing on the Occator dome (Fig. 11), and can be either buried by bright material deposition or broken down by dome collapse or subsequent regolith formation. Occator may be a peculiar case involving a small circular central circular depression producing an easily recognized circular dome, whereas other pits on Ceres of different sizes and shapes may have produced more distributed styles of deformation on the pit floors. The apparent preservation of domes on Ganymede and Callisto requires explanation but may have to await the advanced instrumentation of future orbiter

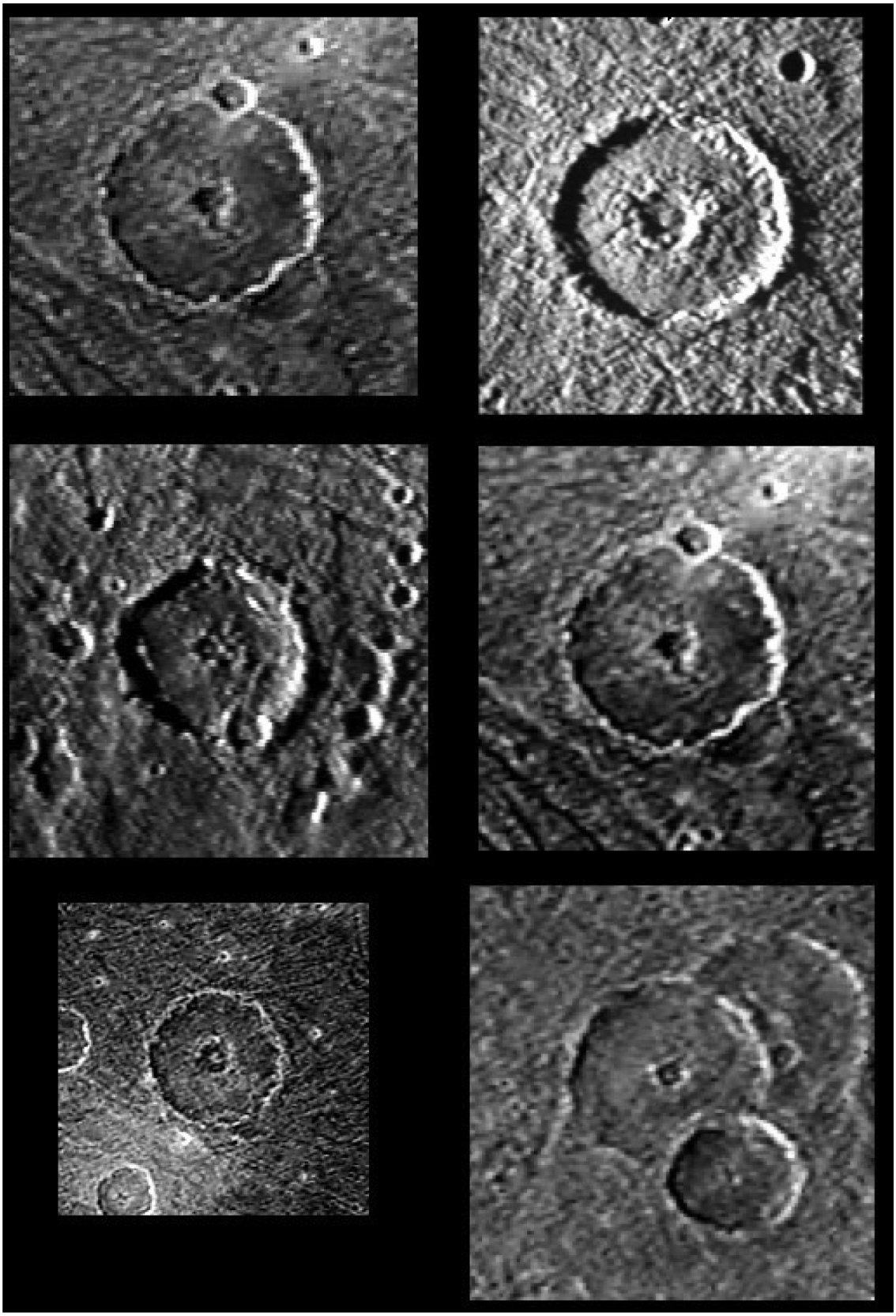

Fig. 19. Voyager images of central dome craters on Ganymede. These craters are all between 60 and 80 km across and were observed at 0.5 to 0.7 km pixel scales. .

missions.

Central domes (and the depressions they sit with) are the nearly ubiquitous central structure in craters >60 km across on Ganymede and Callisto (Schenk, 1993; Schenk et al., 2004). Central domes are thus an integral part of the pit formation process on those bodies and might be so on Ceres, despite the fact only one is observed on within the dozen

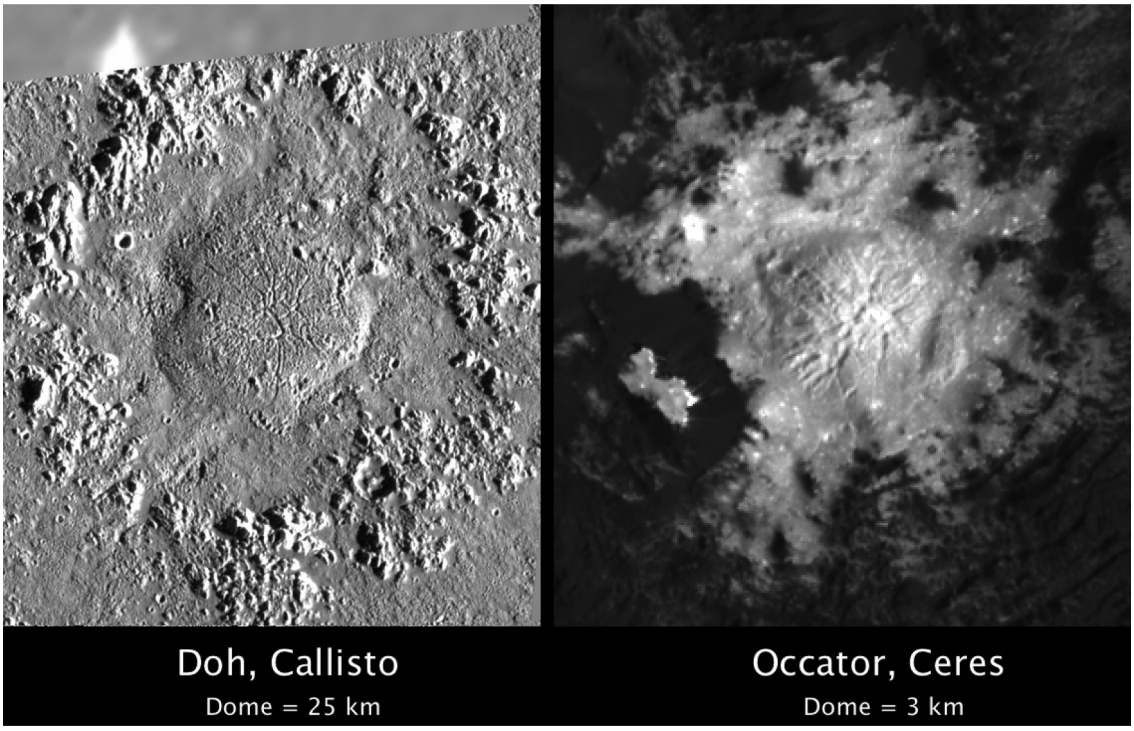

Fig. 20. Comparison of central domes on Callisto (left) and Ceres (right). Note rugged massifs flanking Callisto dome, and differences in scale of domes. Galileo image of Callisto was acquired at 90 m pixel scale, Occator at 35 m pixel scale.

or so central pit craters there. The transition from central pit to central dome craters on Ganymede and Callisto occurs at ~60 km (Schenk et al., 2004). We do not know the transition on Ceres based on only one example (at 92 km) and the fact that several larger craters lack domes, but even this example is much smaller than a predicted crater transition diameter to domes of ~200 km on Ceres if simple g^{-1} scaling of the Ganymede/Callisto examples applies (Fig. 22). This is the one crater morphology that does not scale on Ceres with g^{-1} to its related features on icy moons (Schenk et al., 2016; 2018).

More illuminating is the similar degree of domal surface fracturing on both Ceres and Ganymede and Callisto (Fig. 20), suggesting either fracturing of the surface of an ascending viscous plug (in the manner of terrestrial dacitic or rhyolitic domes), or inflation of the surface from below by either freezing of a shallow lens of water-rich material or laccolithic intrusion from deeper regions (see Quick et al., 2018, this issue). The apparently lack of a termination scarp at the edge of the central dome suggests that it is not an extrusive feature but rather inflated below.

Observations of the dome at Occator indicate that the surface of the bright deposit covers the pit and dome in a contiguous deposit draped

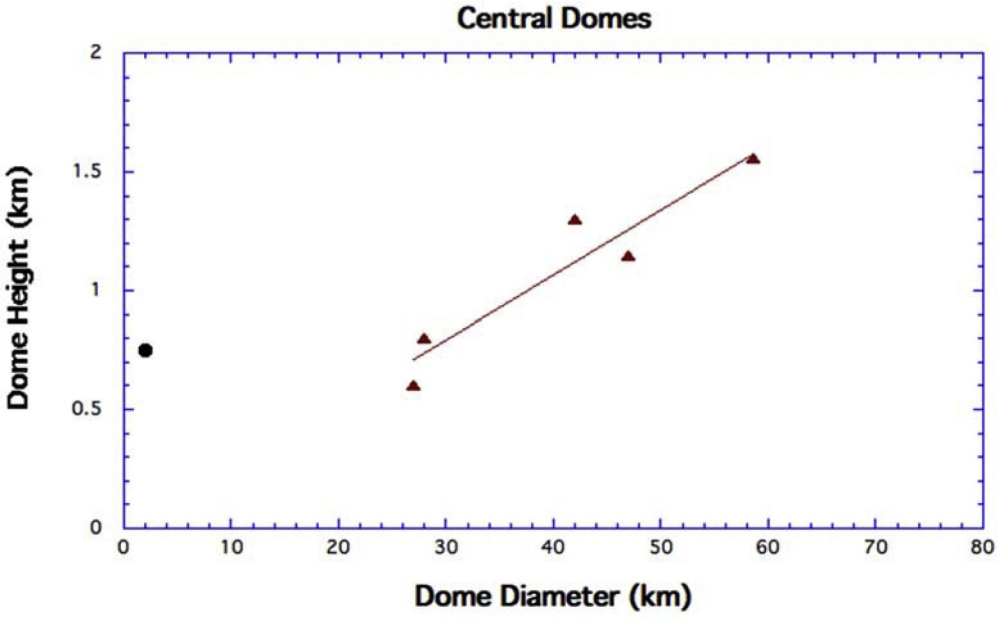

Fig. 21. Heights of central domes as measured at Occator on Ceres (large dot) from Dawn topography and Ganymede (triangles) from Galileo stereo and photoclinometry topography data (this report).

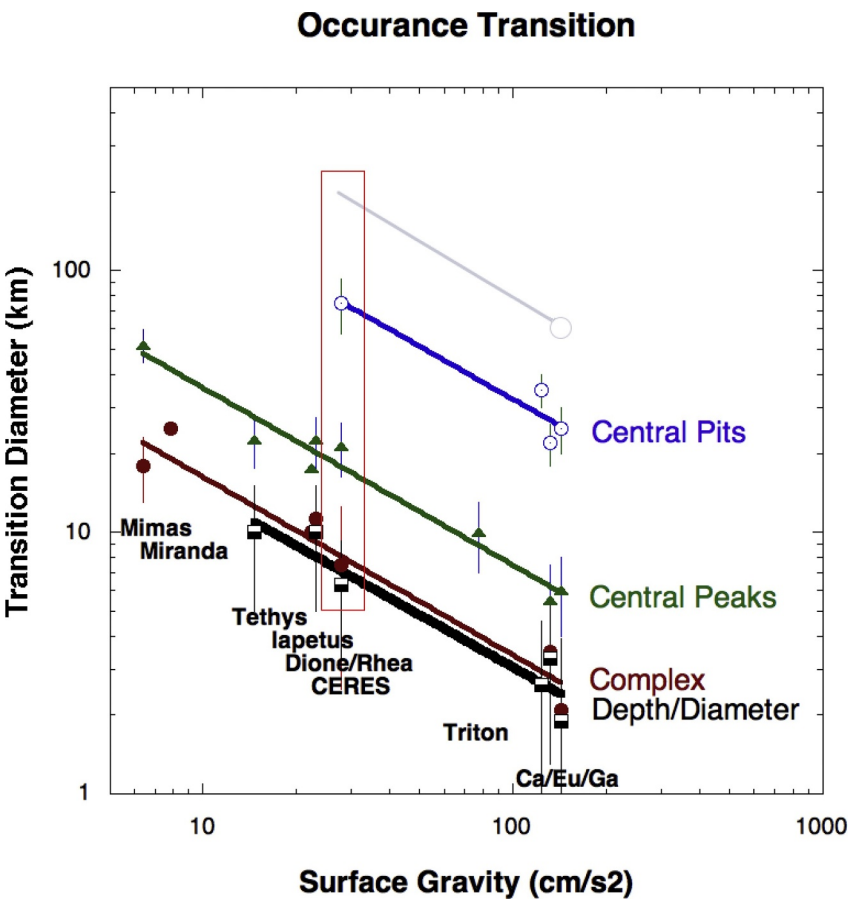

Fig. 22. Transition diameters for complex craters on Ceres and icy satellites. Satellite data from Schenk (1991) and White et al. (2013, 2017) and from this study. Red box highlights Ceres data points. Grey line at top indicates g^{-1} extrapolation of observed central dome transition on Ganymede and Callisto (Schenk, 1993). (For interpretation of the references to color in this figure legend, the reader is referred to the web version of this article.)

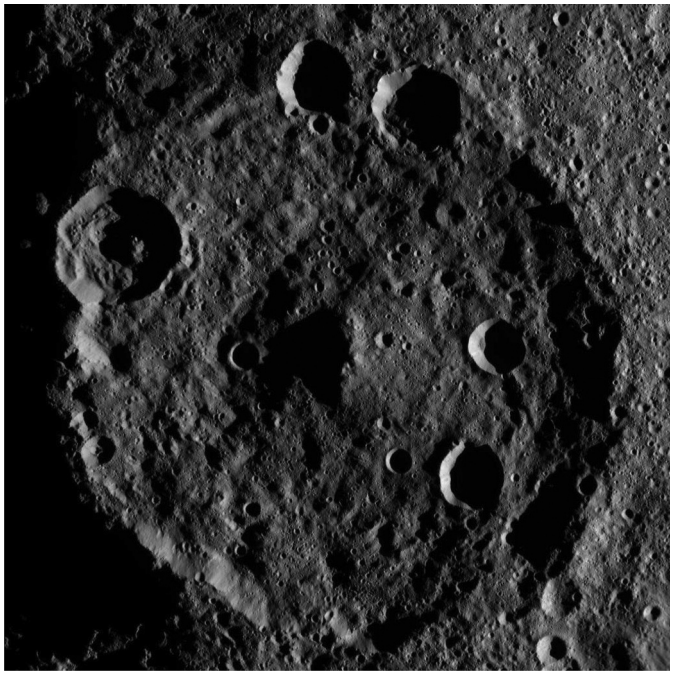

Fig. 23. Dawn view of Zadeni crater, showing large conical central peak that is mostly intact. Crater diameter is ~124 km. Sun is to the right.

over a rugged surface of variable elevation, but that fracturing occurs only on the topographic dome in the center (Fig. 11). There is no evidence in the 35 m/pixel imagery for partial obscuration of earlier generations of fracturing by later depositional sequences, though image resolution may preclude such detection. Further, these is no evidence for materials having been extruded from the fractures on the crest of the dome, implying either high viscosity of subsurface materials or a deposit too thick to penetrate. Thus, fracturing (and likely the uplift itself) occurred after the deposit was completely or nearly completely formed or solidified. Further, we observe no evidence for a topographic marginal scarp to the dome, which rather appears to be a simple upwarping and fracturing of the preexisting surface of the bright deposit without a structural or constructional margin. Viscous extrusive deposits always have a substantial flow front but none are observed here. This implies upwarping of the surface from below, through subsurface inflation (as in a intrusive laccolith) or volume expansion of the subsurface through freezing of water ice, or both.

Laccolithic uplift from below at Occator can explain the formation of the extensive fracturing on the dome crest. Crest fracturing is commonly observed in strata overlying salt domes that have not breached the surface (e.g., Yin and Groshong, 2006, and references therein). These fractures are due to uplift and extension and form a variety of patterns from grid-like to radiating, consistent with the pattern observed at Occator (Fig. 25).

Similar fracture patterns are observed in strata overlying pingos or frost-mounds, including classic fractured examples at Tuktoyaktuk Peninsula, Yukon (e.g., Holmes et al., 1968; Mackay, 1998). Pingos are domical mounds produced by groundwater movement and freezing. They represent a more provocative analog to the Occator central dome in that they involve the forced migration of fluids (i.e., water) during the freeze-thaw cycle often observed in terrestrial polar environments (e.g., Mackay, 1998). This leads to the net accumulation of water due to pore-water expulsion and solute rejection among other processes, which uplifts the ground as it freezes, coupled with the addition of new water forced into the area from below and adjacent areas, resulting in net domical growth. This can be followed by subsequent collapse due to

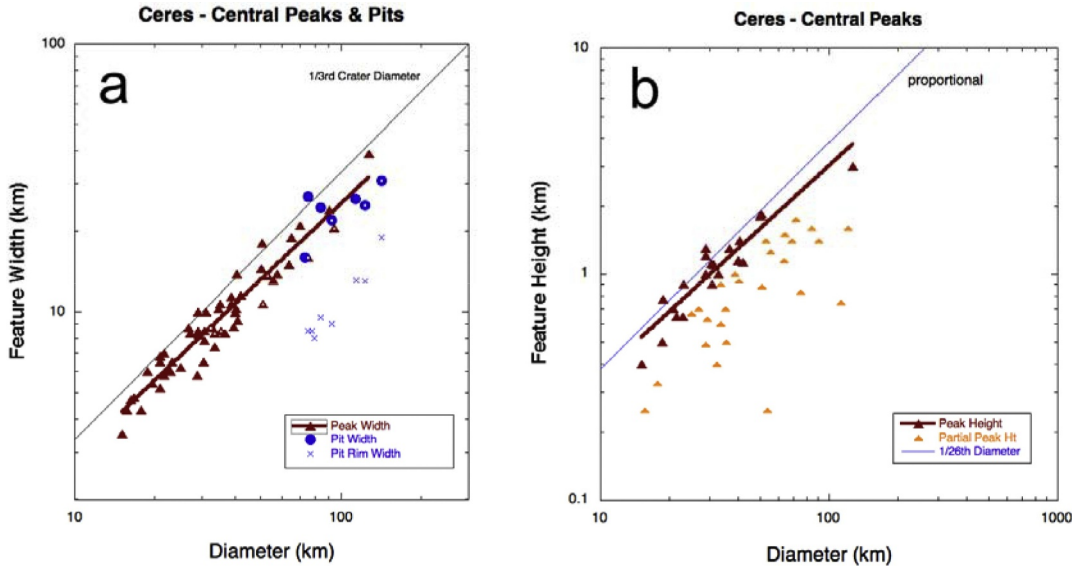

Fig. 24. Widths and heights of central peaks and pit rims on Ceres. Largest peak is from Zadeni crater (Fig. 23). (+) is for the pit rim at Toharu crater and (x) is for the pit rim at Occator, with height being the current observed value for the rim pit.

a variety of factors. Well-preserved fractured domes 10′s of meters across have also been identified on Mars by Dundas and McEwen (2010) and are considered likely pingos or frost-mounds. On Ceres, the terrestrial and martian freeze-thaw cycles may be replaced by a progressive contraction of the hot 'plugs' at the centers of large craters, where water can persist, in which water and solutes are driven out as this sub-crater material freezes radially inward (as described in Bowling et al., 2018, this volume). Any role played by Earth's flora and fauna would not occur on Ceres obviously.

The inferred sequence of central pit formation, followed by bright material deposition and then upwarping and fracturing of the pit floor indicates that the dome within Occator's central pit formed subsequent to the main impact event. This might stand in contrast to Ganymede (and Callisto) central domes which are inferred to form promptly as part of the central uplift and cratering process in general (due to the apparently observation [pending return to Jupiter] that bright ray and floor material also cover the central dome; Schenk, 1993). Crater counts on the surface indication that this could have occurred as late as 3–5 million years after the crater formed (Neesemann et al., 2018, this issue), though there is considerable uncertainty in this estimate, and it is possible that the dome and deposit formed within the timeline suggested by the numerical models (Bowling et al., submitted this issue). Further work is needed to resolve these issues.

No evidence can be identified at Occator that the dome involves extrusion of material onto the surface, but surface extrusion is not required for the ice-lens freezing or intrusive laccolithic model to be valid. The question then becomes whether this sequence is valid for central domes on all icy bodies or is peculiar to Ceres, given that it occurs on Occator at a smaller crater diameter than expected. Water ice is now considered to be a significant but minority species to approximately <35% by volume of the outer layers of Ceres (e.g., Fu et al., 2017). This should be more than abundant enough to migrate and concentrate in the hot central areas of impact craters there (e.g., Bowling et al., 2018). The outer layers of Ganymede are likely mostly water ice, so the migration and freeing of water to produce the dome would have to occur there in the absence of non-ice material. This could occur is temperatures are warm enough to melt water in the centers of craters >60 km across (e.g., Senft and Stweart, 2011; Elder et al., 2012).

Elder et al. (2012) show that the potential volume of liquid water produced and the available pore space are both plausibly sufficient to explain the central pits observed in many craters on Mars and Ganymede/Callisto. They also conclude that they may not be sufficient to produce central pits on mid-sized satellites. They did not address Ceres as no imaging was available in 2012. Field mapping and modeling all indicate that the central uplifts of large craters are the most densely distorted and fractured areas of a crater and likely to be the most porous. Whether they are more permeable is less clear as significant quantities of melt and debris are injected into fractures during the excavation phase in terrestrial craters, potentially choking off drainage

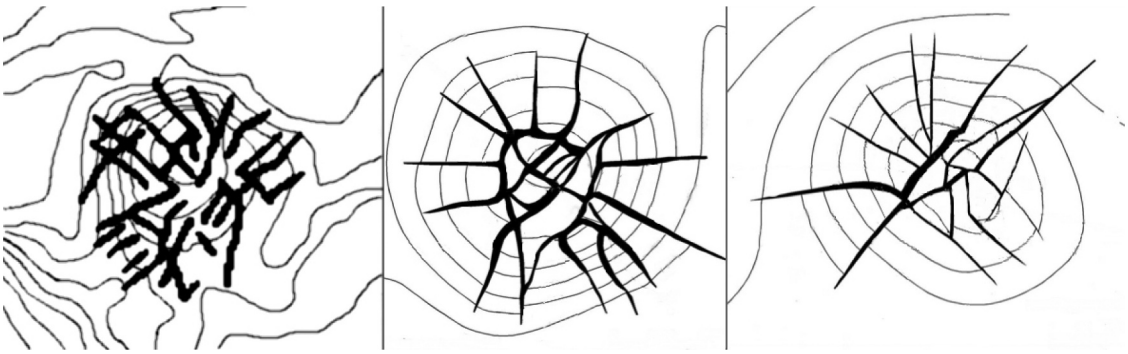

Fig. 25. Sketch maps of fracture patterns on central dome at Occator (left) and surface expression of two subsurface salt domes on Earth. Salt dome maps simplified from Yin and Groshong (2006). Maps show prominent fracture sets in heavy lines, and contours in light lines. Topography on surface in all cases is 500–1500 m. Occator dome is ~3 km wide. Terrestrial salt domes are 1.5 and 3 km wide, respectively. .

paths. Liquid water may behave differently of course.

The central dome observed at Occator may be due to either intrusive uplift or freeze expansion of water accumulated below the surface. If freeze expansion, we can estimate the volume of ice required to form the dome. The volume of the observed dome is ~3.75 km^3, assuming a flat preexisting surface (or as much as doubled if the pit floor was bowl-shaped). Assuming the standard densities for water and ice, we estimate that on the order of 4e12 kg of water must freeze to produce a dome of the observed size. Intruding the 3.75 km^3 of ice may be easier to accomplish. Whether either mechanism is realistic given the observations is open for debate, and further investigation of these and other mechanisms is required.

4.3. Origins of Occator lobate floor-fill materials

Because of the inference that Cerealia Facula formed due to the residual effects of impact heat, it is worth considering the origins of the lobate floor-fill deposits in Occator and other large craters. The evidence for melt flow morphologies (Figs. 3 and 7), the generally flat-lying topography of the unit (Figs. 1 and 2), and the effectively indistinguishable ages of the lobate floor and external ejecta deposits (Neesemann et al., 2018, this issue), all indicate that the lobate floor-fill material is likely a mobile deposit of melted or partially melted crustal materials formed at impact. We consider three models for the origin of this deposit: impact melt, post-impact volcanism and post-impact landslides. In the later case, a proposed location for such a massive landslide would be the steep southeastern rimwall scarp (Nathues et al., 2018, this issue).

Models of large impact into low gravity bodies of Ceres' likely composition at Ceres mean impact velocity of ~ 5 km/s (e.g., Bowling et al., 2018; this issue) indicate that maximum temperatures are not sufficient to melt silicates but are sufficient to melt water ice and that this will occur mostly along the outer surface of the forming crater cavity and in the center of the crater. Current best models for Ceres indicate that large impacts occur in a mixed outer layer composed of hydrated Mg- and ammoniated- phyllosilicates, Mg-Ca-carbonates, water ice and salts (De Sanctis et al., 2015; Ammannito et al., 2016; Carrozzo et al., 2018; Combe et al., 2016; Sizemore et al., 2017; Prettyman et al., 2016). Thus any impact melt on Ceres would consist of an admixture of water with suspended and dissolved particulate silicates, salts and carbonate materials, forming a sort of "impact mud." Whether impact heating is sufficient to produce large quantities of melt some time after impact or deep beneath the crater depends strongly on input variables, including the hypothesized thermal, physical and chemical pre-impact state of the interior at the Occator site.

The impact models (Bowling, et al., this issue) indicate melting will occur mostly along the surface of the expanding crater cavity and in the central region, and can be expected to line the final crater surface. While locally ponded deposits of lobate floor-fill material are visible in scattered regions throughout much of the floor of Occator (Figs. 4–6), we observed extended contiguous deposits covering large areas only to the south and east (Figs. 1, 2 and 7). These indicate that melting did not occur uniformly within Occator, or that the southeast crater floor was lower and most of the melt material ponded there instead of a higher standing northwestern sector.

Impact melt, being a molten rock formed relatively early in the impact process, will respond as a fluid to the dynamically changing crater floor topography ("floor" in this case referring to the unmelted but highly fractured basement beneath the melt sheet). The melt deposits that lined the expanding crater cavity will tend to flow downslope inward into a crater center that is rapidly changing in relief and elevation. Some of these melt deposits will then be trapped or ponded in contemporaneously forming local closed topographic depressions such as the tops of terrace blocks (e.g., Tornabene et al., 2012; Hawke and Head, 1977), as is seen on craters like Tycho, and in Occator itself (Figs 4–6), but most will concentrate onto the depressed crater floor to pond in a large contiguous deposit, embaying ridges and high-standing knobs as it settles and solidifies.

Further, the contemporaneous central uplift will cause melt deposits near crater center to be displaced outward, at least partially, creating potentially confusing flow direction indicators on the crater floor. Melt deposits may override deposits emplaced only a short interval before. In any case, the surface expression will be one of distributed refrozen molten rock units flowing in multiple directions. Smaller-scale downslope flow deposits are often observed in high-resolution images of terraces and floor units of fresh lunar craters (e.g., Hawke and Head, 1977) as well as at Occator (Fig. 6). These also resemble low-viscosity silicate lava, but are interpreted as impact melt draped on terraces and the ejecta deposits.

In many ways, an impact melt sheet and associated deposits can be considered a form of instantaneously formed volcanic-debris avalanche due to its emplacement conditions, and will share some of the characteristics of both volcanic flows, as evidenced from high-resolution views of lunar impacts, as well as massive debris avalanches. Thus, impact melt should share many flow characteristics and behaviors in common with silicate lavas, and can thus be easily confused with such. The major differences between impact melt and classical volcanism, are that impact melt lacks a deep root or source vent for extrusion (being a surface deposit that forms instantaneously and lines the expanding impact cavity during formation) or a unique source localized scarp (for giant landslides), and is distributed over much, if not all, of the crater interior in variable quantities. (An impact melt deposit on Ceres could also be superheated relative to a volcanic material of similar composition, though it is not known what the effects of this might be.) Based on the similarity at Occator and large lunar craters of surface textures (Fig. 7) and ponded lobate floor-fill material in Occator in small topographic lows across much of the crater floor at a wide range of elevations (Figs. 4–6), and the effectively equivalent surface ages of the crater floor and the ejecta deposits at Occator (Neesemann et al., 2017) we conclude that the lobate floor-fill deposit at Occator is an impact melt deposit formed contemporaneously with the excavation of the impact crater.

The perching of small outlier units of lobate floor material at widely divergent topographic elevations up to 1000 m or more above the crater floor over most of the crater surface (Figs. 8–10) is difficult to reconcile with either post-impact volcanism or giant landslides, regardless of when they occurred. These smaller pockets are often observed to connect with the main floor deposit via downslope flow lobes, indicating that the local deposits are both contemporaneous and contiguous with the main deposit, again inconsistent with either volcanism or a giant landslide. Such features are observed in Martian and lunar craters (e.g., Tornabene et al., 2012; Hawke and Head, 1977). Further, there is also no evidence for constructional edifices within any of the lobate floor materials, despite its evident relatively high viscosity. While post-impact extrusion of viscous lavas cannot be excluded from available evidence, the perching of small outcrops of this material on terrace scarps around the circumference of Occator and the lack of central edifices suggest that volcanism in the classical sense is not the most likely explanation.

Similarly, the perching of stranded outcrops along most of the circumference, and the large lateral extent of the deposit far from the hypothesized southeast rimwall source scarp, also argue against the giant static landslide hypothesis, but can be explained as a mobile mixed debris-melt deposit formed across much of the crater cavity. The wide distribution of exposures of this material in topographic lows, including on the crater floor and at smaller sites where perched on isolated topographic benches like terrace blocks (Figs. 8 and 9), is very easily explained as stranded pockets of impact melt, the excess of which flowed downslope and accumulated at crater bottom. The available evidence favors a formation mechanism that produces a fluidic and mobile deposit over most of the crater floor contemporaneous with impact, namely impact melt.

The greatest relief along the margin of the lobate deposits is along the northern margin, where it overlaps deep depressions and high massifs (Fig. 3b). Elsewhere the deposit has low relief along its margins of meters to 10s of meters (Figs. 4 and 5). This gradient in marginal relief correlates with the observed northward gradient in the increase in deposit ruggedness (e.g., Scully et al., 2018, this issue; this report). These two observations suggest that the apparent viscosity and/or yield strength of the deposit increased northward, perhaps in correlation with the direction of flow as the melt sheet slid back into the deep cavity of the forming crater possibly from the southeast. We also speculate that greater amounts of fragmented solid debris may have accumulated at the bottom of the crater, increasing the effective viscosity of the flow in those areas.

Further, the similar knobby and ropey surface textures of the lobate floor-fill material in Occator and the Tycho impact melt sheet (Fig. 7) likely come from distortion of the chilled surface crust during ongoing lateral flow as well as abundant unmelted fragmental debris, which became entrained in this deposit as it was dynamically emplaced. Impact melt is often choked with significant fractions of solid fragmented impact debris (this type of mixed breccia/melt material is common in large terrestrial impact sites). Some of the knobs observed within the Occator lobate material deposits are likely larger such fragments, or extrusions or upwarping of material from beneath the solid crust of the deposit.

A large ponded melt sheet a hundred or more meters thick on the floor of Occator would be emplaced essentially instantaneously and remain at high temperatures for a significant period of time. Such a deposit might be expected to undergo geochemical processing as it slowly cools and refreezes (e.g., Abramov et al., 2012). Impact melt sheets at Sudbury and Manicouagan (e.g., Simonds et al., 1976; Onorato et al., 1978; Dence, 1972) have undergone significant differentiation but both involve extensively melted silicates and other continental rock types. Impact modeling for Ceres (Bowling et al., 2018, this issue) currently indicates only water ice will melt. The outer layers of Ceres are considered to be no more than 30% water ice (e.g., Fu et al., 2017), and due to the inferred rapid shearing during excavation and emplacement, this melted water will be intimately mixed with particulate and fragmental debris and can react with it. We do not attempt to model geochemical evolution within this deposit but postulate that a variety of reactions will occur as the deposit equilibrates and cools, including exsolution of new phases, exsolution of water ice as freezing occurs, settling or floating of large fragments as they solidify, depending on relative buoyancy, among other effects. These processes should produce local upwellings, ventings, and disturbances on the freezing outer crust, which may be visible as small pitting, maar-like depressions, folds, and crenulate textures on the surfaces of the Tycho and Occator melt sheets, in addition to those produced by lateral movement during deposit emplacement.

A large impact melt deposit on the floor of Occator might also be expected to undergo physical processing as it cools. The deposit will likely freeze from the top and bottom. The silicate fraction might undergo cooling contraction, while the water fraction might undergo freeze expansion. The weight of the solid crust may increase the pressure within the still partially molten interior, leading to possible extrusions of molten material on the surface. The outer crust of the deposit will no doubt be fractured and become uneven as solidification proceeds.

4.4. Origins of bright materials and hydrothermal deposition within Occator

The identification of salts and Na-carbonates in association with the bright spots at Occator has led to suggestions that these deposits formed by a process analogous to hydrothermal deposition of precipitates (e.g., Dombard et al., 2015; De Sanctis et al., 2016; Quick et al., this issue). Indeed, hydrothermal alteration of rocks are noted in terrestrial craters (e.g., Arp et al., 2013) and postulated for Martian craters (Barnhart et al., 2010; Osinski et al., 2013). Residual impact heat is a well-known phenomenon and is always most intense and prolonged in crater center (e.g., Barnhart et al., 2010; Bowling et al., 2018; this issue).

The detailed morphology of Cerealia Facula in Occator at 35 m pixel scales, specifically the downslope tendrils and small sub-kilometer bright spots on the outer edges, are not inconsistent with hydrothermal deposits on Earth. In cases where hot springs create travertine or other carbonate rich deposits, they frequently form in depressions due to the fact that the fluids containing the dissolved minerals will flow to local topographic lows. Examples include the Huanglong Springs in north-central China, Mammoth Hot Springs, CA, and Semuc Champey in Guatemala. These deposits often occur as travertine terraces in river valleys, which are not necessarily expected on Ceres due to the lack of an atmosphere. If hydrothermal deposits form due to precipitation of dissolved species in warm fluids, the exposure of this fluid to space will likely lead to rapid vaporization and perhaps spray of mineral-heavy fluids or crystals on Ceres (e.g., Quick et al, submitted this issue). How this will be manifest at meter scales is not clear, and is not resolved in the Dawn images.

More massive examples of hydrothermal deposits on Earth include the Grand Prismatic Springs at Yellowstone, which forms a large tabular and terraced deposit meters to hundreds of meters thick. In other cases, individual source vents produce narrow stream-like conduits that radiate outward, such as at Witjira-Dalhousie Springs (Fig. 26) in south-central Australia (Wolaver et al., 2013; Clarke and Bourke, 2011), a series of >25 hotsprings concentrated in a ~5 by 10 km wide region of South Australia (Fig. 26).

We postulate a scenario for the central bright deposits on Occator that, despite the obvious differences in environmental and compositional conditions at Ceres and South Australia, may be to first order related. Some of the sinuous traces of the bright spots within the central depression at Occator on Ceres could be mineral precipitates accumulated by repetitive or continuous outflow from small vents along the sides of the central depression (Fig. 27). Small bright spots and several of the sinuous downslope bright tendrils along the western margins of the central pit at Occator appear to emanate from discrete horizontal ridges or outcrops in the 35 m/pixel resolution images (Fig. 27).

Fig. 26. Witjira-Dalhousie Springs, Australia. Image acquired from Google maps with alteration.

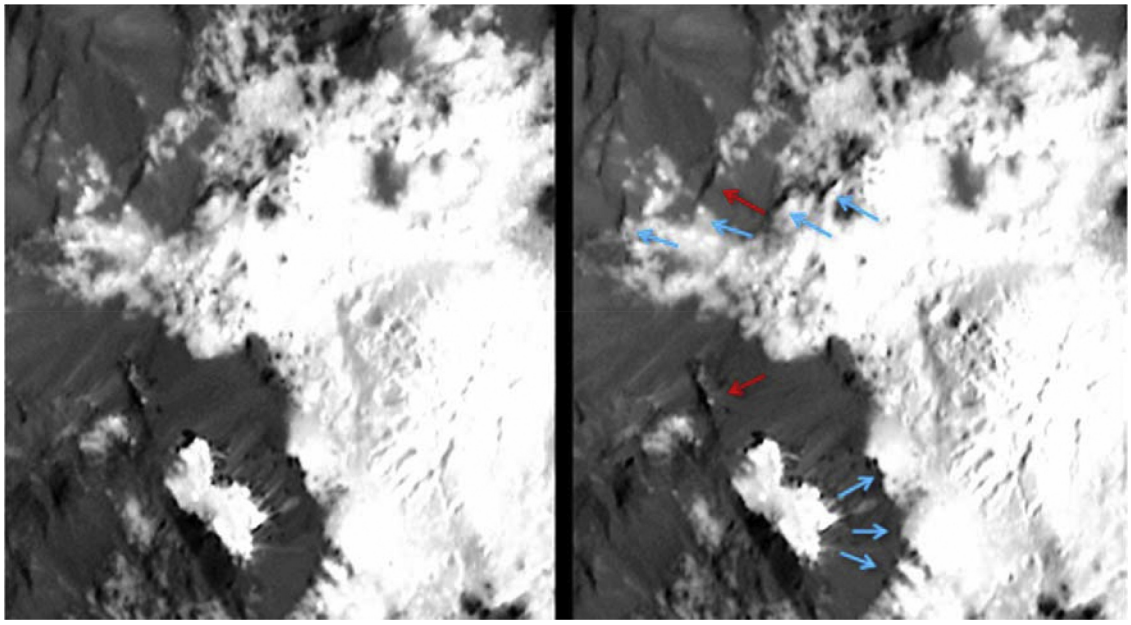

Fig. 27. Enlargement of 35 m resolution map of Occator central pit ((with annotation at right). Arrows indicate apparently horizontal scarps or ridges. Bright material appears to emanate from several of these features, which may be sources for groundwater seepage or other outgassing of material. .

Whether these features represent sources of generalized venting of hydrothermal fluids is provocative but represent the most direct indications of such in the global mapping data.

As the central pit is both amongst the lowest topography in the crater and the area where residual heat is highest and longest lasting and melting of subsurface ice most concentrated (Bowling et al., 2018, this issue), the site of abundant subsurface groundwater from the failed central peak (if our preferred hypothesis for the pit is correct), and the area of the crater floor likely to be most densely fractured and permeable (e.g., Wilson and Stearns, 1968; Milton et al., 1972; Wilshire et al., 1972; Kenkmann, 2002), it is plausible that hydrothermal fluids could be recycled and would escape along the most permeable fracture systems in the central depression.

The rounded ends of the fingerlike projections associated with the central bright deposits located on the upslope outer walls of the central pit (Figs. 8 and 9) could be derived from individual sources. Some of these deposits extend onto the fractured lobate floor-fill deposits along the outer margin of the central pit (Fig. 8), indicating that deposition of the salts and carbonates occurred after the upper surface of the lobate floor-fill deposits had essentially crystalized. Otherwise, the bright mineral deposits form in local lows as the fluids flow short distances downslope as they flash evaporate to space, leaving local highs essentially uncovered and relatively dark (Figs. 8 and 9). At Occator, the outlets are in the central depression and flow inward, whereas at Dalhousie, Mammoth and Yellowstone, they tend to form a central cluster and radiate outward, due to local topography, some of it constructed from hydrothermal deposition.

Whether the observed Occator deposits result from simple outflow onto the surface or highly localized fountaining of spray at the source (e.g., Quick, submitted this issue) is unclear, but the finger-like morphologies at the edge of the deposit suggest that it was not emplaced by one large central fountain or geyser of activity which would tend to coat the entire pit wall (unless downslope movement of dark material is eating away at the margins of a once larger deposit). Such a scenario could explain the presence of localized deposits of bright material atop isolated mesas (Figs. 8, 9 and 11), which would otherwise require local venting sources at those sites. In short, the morphology of the bright deposit at Cerealia Facula presents ambiguous indications regarding emplacement, and could require both construction and destruction to explain.

The estimated crater retention age of Cerealia Facula of several million years later than the formation of the crater, if taken at face value, suggest that the bright deposit could have formed some time after impact. Bowling et al. (2018, this issue) model impact heating and find that it could last up to ~1 million years after impact. Dombard et al. (2015) also investigated residual heat and suggest that significant heating could last 0.1–10 million years after impact in a near-vertical impact, perhaps sufficient to account for the differences in measured crater densities and inferred ages. The longevity of a liquefied subsurface impact related mass could also be prolonged depending on the concentration of dissolved materials. We do not further address these issues here except to note uncertainties in age dating, the duration of residual impact heat, and the composition of subsurface fluids.

4.5. Temporal change at Cerealia Facula, Occator crater

Finally, a useful constraint on the origins of Cerealia Facula is whether the bright deposits are actively forming or being modified in the current epoch. As the deposits were not resolved before Dawn arrival we can ascertain changes only between 2015 and today. If the deposits are only a few million years old or less, they could simply be well preserved, and indeed we so no evidence for significant regolith development on the site. Nonetheless, the preservation of the site and the likelihood of residual impact heat being at least partly responsible for the activity there allow that some late stage activity could be occurring today.

Active changes at Cerealia Facula could be sudden, such as landslides on the pit rim or within the central dome, or outbursts or eruptions of fluids at new or long dormant sites from a subsurface reservoir, among others. Slow change could include intermittent low-level venting of fluids from existing source vents or slow creep of surface materials. The Dawn mission observed the Cerealia Facula deposit at resolvable pixel scales (<500 m/pixel) from DOY 160(2015), to DOY 292(2016), over a period of 497 days (Fig. 28), or ~0.3 Ceres orbit. Despite parallax shifting between many frames, no recognizable changes in the shape or surface patterns of the Cerealia Facula bright deposit were detected over that period, in the constraint of changing resolution (35 to 410 m/pixel) as the spacecraft moved from its early distant orbits into its closest orbit and then back out to greater distances over this period. Additional observations were acquired before and

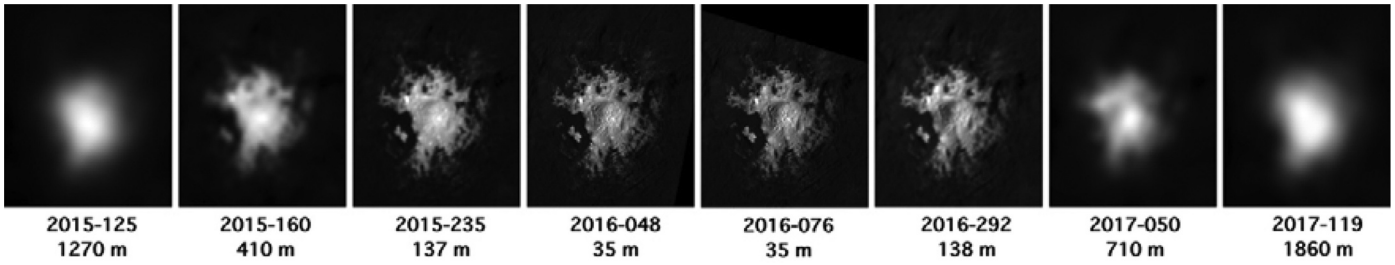

Fig. 28. Dawn observations of Cerealia Facula, Occator, over a period of nearly 2 years in 2015–2017, illustrating the lack of major changes at this structure. Pixel scale resolutions are shown below the year and day-of-year of the observation.

after this period at DOY 125(2015), and 50(2017) and 119(2017) at resolutions of 700 to 1900 m/pixel (Fig. 28), or ~0.4 Ceres year, but these are sufficient to show only the coarsest of changes, of which none are resolved. These observations would strengthen arguments that the occasional observed volatile outbursts at Ceres (Kueppers et al., 2014) are correlated with solar flare impacts with Ceres (Villarreal et al., 2017) and not surface geologic activity.

Surface changes involving slow percolation of fluids and subtle local changes to surface brightness may not have been directly observable by Dawn. No photometric study was attempted here but sun direction was consistently from the east in this time period (though Solar elevation did fluctuate between 25° and 60° in most cases) and no major brightness changes are evident within the deposit or along its margins in the observations (Fig. 28). Observations over a range of phase angles from ~1° to 102° (Fig. 29) also show that the bright deposits remain bright over all observed phase angles. While the Dawn mapping period is too short to constrain all possible modes of activity, such as slow percolation of fluids from existing vents, these observation do suggest that large-scale major or rapid changes have not been occurring, or that activity had been continuous throughout the period resulting in no change in surface patterns.

5. Discussion and conclusions

Mapping of Ceres by the Dawn spacecraft reveals that central pit craters dominate at diameters >70–75 km on Ceres, and that the bright deposit at the center of the young 92 km crater Occator is associated with both a central pit and a fractured central dome. A key constraint is the absence of central pits on similarly sized icy moons of Saturn and Uranus where surface and internal temperatures are colder but the ubiquitous presence of both central peak and central dome craters at D > 30 km on larger Ganymede and Callisto. These and other observations tend to support models wherein central peaks form in a partially or largely molten state, depending in part on latitude (as related to subsurface temperatures). However, none of the current hypotheses for pits or domes fully satisfy the observations, suggesting that either the models need to be improved in terms of physical completeness or realism, or new models are required.

Assuming the molten peak hypothesis is indeed reasonably correct, much remains to be understood in terms of the fate of the missing central peak material. For example, is the proto-central peak all liquid or only partly so, as is general crustal material on Ceres, where does the missing mass go? If peak failure (by whatever mode) occurs, why does the crater end up with a small depression or a remnant peak instead of a large pile of disaggregate debris? Despite these ambiguities, the new observations at Ceres thus provide key constraints as attempts are made to improve the physical realism of numerical impact models on Ceres and the icy moons of Jupiter, Saturn and Uranus.

Similarly, the origin and fate of the central dome at Occator remains only partly understood. Dawn mapping observations at 35 m pixel scales indicate that the dome may be due to inflation of surface from below and that the domed topography post-dates bright deposit formation, but at these scales we could be missing diagnostic features. Why is there only one central dome on Ceres despite the observation of ~11 additional though older central pit craters? Are the ubiquitous central domes on Ganymede and Callisto related by similar formation processes, as the prevalence of fractures on their surface would suggest, or is this a false lead?

The origin of the bright deposits of Cerealia Facula is likely linked to hydrothermal fluids created and mobilized by the impact (e.g., De Sanctis et al., 2016). Slowly decaying impact heating may have been sufficient to drive these fluids to the surface, and while mobilization of preexisting deep brine layers or pockets have been postulated (e.g., Stein et al., submitted this issue; Nathues et al., submitted this issue) we see no direct evidence that compels such an interpretation.

The 35 m pixel scale Dawn observations provide the best look at central pit craters and a central dome on ice-rich targets (other than Mars), and provide a key test and/or prediction for what we might

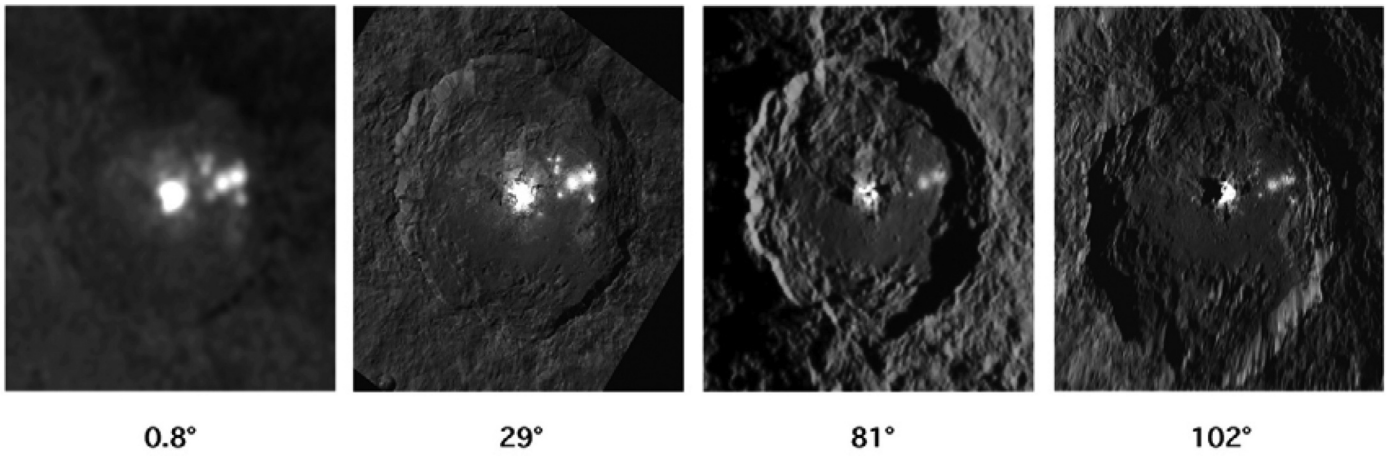

Fig. 29. Occator crater (D = 92 km) over a range of phase angles. Resolutions range from 35 to ~1900 m/pixel.

expect to observe once we acquire comparable high resolutions on Ganymede and Callisto in the 2020s. It will then be necessary to target the freshest central pit craters (i.e., those with bright rays) to search for debris or flow patterns that might confirm, refine or refute the peak melt hypothesis.

Calculations indicate that at typical impact velocities, comparatively little impact melt will be generated or retained on large asteroids (Keil et al., 1997; Bowling et al., 2018, this volume). Hydrated silicates were not modeled by Keil et al. explicitly but were inferred to be even more difficult to melt. On the other hand, for the ice-rich mixture relevant to Ceres' crust, both Dombard et al. (2015) and Bowling et al. (2018, this issue) found that sufficient heat was produced to melt the available ice and produce what presumably would be an impact-derived water-rock slurry melt, or 'impact mud.' As no other low-melting point candidate material is available in large quantities on Ceres, the formation of large deposits of flat-lying impact melt at Occator and other large craters such as Ikapati and Dantu that embay low areas, and formation of central pits by melting of uplifted materials, would imply that the upper layers of Ceres are indeed composed of significant amounts of water ice, and are part of a suite of features (e.g., Schmidt et al., 2017; Ruesch et al., 2016) that betray the presence of water ice on Ceres.

Acknowledgments

We thank Veronica Bray and Elizabeth Silber for their comments and suggestions on the manuscript. We also thank the Dawn Participating Scientist Program for its support.

Supplementary materials

Supplementary material associated with this article can be found, in the online version, at doi:10.1016/j.icarus.2018.08.010.

References

Abramov, O., Wong, S.M., Kring, D.A., 2012. Differential melt scaling for oblique impacts on terrestrial planets. Icarus 218 (2), 905–916. https://doi.org/10.1016/j.icarus.2011.12.022.

Alzate, N., Barlow, N.G., 2011. Central pit craters on Ganymede. Icarus 211 (2), 1274–1283.

Ammannito, E., De Sanctis, M.C., Ciarniello, M., Frigeri, A., Carrozzo, F.G., Combe, J.-Ph., Ehlmann, B.L., Marchi, S., McSween, H.Y., Raponi, A., Toplis, M.J., Tosi, F., Castillo-Rogez, J.C., Capaccioni, F., Capria, M.T., Fonte, S., Giardino, M., Jaumann, R., Longobardo, A., Joy, S.P., Magni, G., McCord, T.B., McFadden, L.A., Palomba, E., Pieters, C.M., Polanskey, C.A., Rayman, M.D., Raymond, C.A., Schenk, P.M., Zambon, F., Russell, C.T., 2016. Distribution of phyllosilicates on the surface of Ceres. Science 353 (6303). https://doi.org/10.1126/science.aaf4279. id.aaf4279.

Arp, G., Kolepka, C., Simon, K., Karlus, V., Nolte, N., Hansen, B., 2013. New evidence for persistent impact-generated hydrothermal activity in the Miocene Ries impact structure, Germany. Met. Planet. Sci. 48, 2491–2516.

Barlow, N., Ferguson, S., Horstman, R., Maine, A., 2017. Comparison of central pit craters on Mars, Mercury, Ganymede, and the Saturnian satellites. Met. Planet. Sci. 52, 1371–1387.

Barnhart, C., Nimmo, F., Travis, B., 2010. Martian post-impact hydrothermal systems incorporating freezing. Icarus 208, 101–117.

Bland, M., Raymond, C.A., Schenk, P.M., Fu, R.R., Kneissl, T., Pasckert, J.H., Hiesinger, H., Preusker, F., Park, R.S., Marchi, S., King, S.D., Castillo-Rogez, J.C., Russell, C.T., 2016. Composition and structure of the shallow subsurface of Ceres revealed by crater morphology. Nat. Geosci. 9, 538–542. https://doi.org/10.1038/ngeo2743.

Bray, V., Schenk, P., Melosh, H.J., Morgan, J., Collins, G., 2012. Ganymede crater dimensions – implications for central peak and central pit formation and development. Icarus 217, 115–129.

Bowling, T., Ciesla F., Davison T., Scully J., Castillo-Rogez J. and Marchi S., 2018. Post-Impact Thermal Structure and Cooling Timescales of Occator Crater on Asteroid 1 Ceres, Icarus, this issue, in press.

Buczkowski, D, Schmidt, L.,B.E., Williams, D.A., Mest, S.C., Scully, J.E.C., Ermakov, A.I., Preusker, F., Schenk, P., Otto, K.A., Hiesinger, H., O'Brien, D.P., Marchi, S., Sizemore, H., Hughson, K., Chilton, H., Bland, M.T., Byrne, S., Schorghofer, N., Platz, T., Jaumann, R., Roatsch, T., Sykes, M.V., Nathues, A., DeSanctis, M.C., Raymond, C.A., Russell, C.T., 2016. The geomorphology of Ceres. Science 353, 6303. https://doi.org/10.1126/science.aaf4332.

Buczkowski, D.L., Williams, D.A., Scully, J.E.C., Mest, S.C., Crown, D.A., Schenk, P.M., Ermakov, A.I., Jaumann, R., Roatsch, T., Preusker, F., Platz, T., Nathues, A., Hoffmann, M., Schaefer, M., Marchi, S., De Sanctis, M.C., Raymond, C.A., Russell, C.T., 2017. The geology of the Occator quadrangle of Dwarf Planet Ceres: floor-fractured craters and other geomorphic evidence of Cryomagmatism. Icarus. https://doi.org/10.1016/j.icarus.2017.05.025. In Press.

Carrozzo, F.G., De Sanctis, M.C., Raponi, A., Ammannito, E., Castillo-Rogez, J.C., Ehlmann, B.L., Marchi, S., Stein, N., Ciarniello, M., Tosi, F., Capaccioni, F., Capria, M.T., Fonte, S., Formisano, M., Frigeri, A., Giardino, M., Longobardo, A., Magni, G., Palomba, E., Zambon, F., Raymond, C.A., Russell, C.T., 2018. Nature, formation and distribution of carbonates on Ceres. Sci. Adv. 4, e1701645 Under review.

Ciarniello, M., De Sanctis, M.C., Ammannito, E., Raponi, A., Longobardo, A., Palomba, E., Carrozzo, F.G., Tosi, F., Li, J.-Y., Schröder, S.E., Zambon, F., Frigeri, A., Fonte, S., Giardino, M., Pieters, C.M., Raymond, C.A., Russell, C.T., 2017. Spectrophotometric properties of dwarf planet Ceres from the VIR spectrometer on board the Dawn mission. Astron. Astrophys. 598, A130. https://doi.org/10.1051/0004-6361/201629490.

Clarke, J.D.A., Bourke, M.C., 2011. Travertine and tufa from Dalhousie springs (Australia)—implications for recognizing Martian Springs. In: Geol. Soc. Am. Spec. Paper. 2011. 483. pp. 231–247. https://doi.org/10.1130/2011.2483(15).

Combe, J.-P., McCord, T.B., Tosi, F., Ammannito, E., Carrozzo, F.G., De Sanctis, M.C., Raponi, A., Byrne, S., Landis, M.E., Hughson, K.H.G., Raymond, C.A., Russell, C.T., 2016. Detection of local H_2O exposed at the surface of Ceres. Science 80, 353–355. https://doi.org/10.1126/science.aaf3010. aaf3010-1-aaf3010-6.

Croft, S., 1983. A proposed origin for palimpsests and anomalous pit craters on Ganymede and Callisto. In: Proc. Lunar Planet. Sci. Conf., 14th, Part I, J. Geophys. Res. 88. pp. B71–B89.

De Sanctis, M.C., Ammannito, E., Raponi, A., Marchi, S., McCord, T.B., McSween, H.Y., Capaccioni, F., Capria, M.T., Carrozzo, F.G., Ciarniello, M., Longobardo, A., Tosi, F., Fonte, S., Formisano, M., Frigeri, A., Giardino, M., Magni, G., Palomba, E., Turrini, D., Zambon, F., Combe, J.-Ph., Feldman, W., Jaumann, R., McFadden, L.A., Pieters, C.M., Prettyman, T., Toplis, M., Raymond, C.A., Russell, C.T., 2015. Ammoniated phyllosilicates with a likely outer Solar System origin on (1) Ceres. Nature 528 (7581), 241–244. https://doi.org/10.1038/nature16172.

De Sanctis, M.C., Raponi, A., Ammannito, E., Ciarniello, M., Toplis, M.J., McSween, H.Y., Castillo-Rogez, J.C., Ehlmann, B.L., Carrozzo, F.G., Marchi, S., Tosi, F., Zambon, F., Capaccioni, F., Capria, M.T., Fonte, S., Formisano, M., Frigeri, A., Giardino, M., Longobardo, A., Magni, G., Palomba, E., McFadden, L.A., Pieters, C.M., Jaumann, R., Schenk, P., Mugnuolo, R., Raymond, C.A., Russell, C.T., 2016. Bright carbonate deposits as evidence of aqueous alteration on (1) Ceres. Nature 536 (7614), 54–57. https://doi.org/10.1038/nature18290.

Dence, M.R., 1972. Meteorite impact craters and the structure of the Sudbury Basin. In: New Dev. Sudbury Geol. Geological Association of Canada Special Paper. 10. pp. 117–124.

Dombard, A., Saman, K., Schenk, P., 2015. Post-impact cryovolcanism and the bright spots on Ceres. Bull. Am. Astron. Soc. 47 abstract, id.212.08.

Dundas, C., McEwen, A., 2010. An assessment of evidence for pingos on Mars using HiRISE. Icarus 205, 244–258.

Elder, C., Bray, V., Melosh, H.J., 2012. The theoretical plausibility of central pit crater formation via melt drainage. Icarus 221, 831–843.

Engelhardt, W,v., Matthai, S.K., Walzebuck, J., 1992. Aranguainha impact structure, Brazil, I, The interior part of the uplift. Meteoritics 27, 442–457.

Fu, R., 12 others, 2017. The interior structure of Ceres as revealed by surface topography. Earth Planet. Sci. Lett. 6, 153–164.

Goossens, S., Sabaka, T., Genova, A., Mazarico, E., Nicholas, J., Neumann, G., 2017. Evidence for a low bulk density for Mars from gravity and topography. Geophys. Res. Lett. 44. https://doi.org/10.1002/2017GL074172.

Greeley, R., Fink, J.H., Gault, D.E., Guest, J.E., 1982. Experimental simulation of impact cratering on Icy satellites. In: Morrison, D. (Ed.), Satellites of Jupiter. University Of Arizona Press, pp. 340–378.

Hayne, P., Aharonson, O., 2015. Thermal stability of ice on Ceres with rough topography. J. Geophys. Res. 120, 1567–1584. https://doi.org/10.1002/2015JE004887.

Hawke, B.R., Head, J.W., 1977. Impact melt on lunar crater rims. In: Roddy, D.J., Pepin, R.O., Merrill, R.B. (Eds.), Impact and Explosion Cratering. Pergamon Press, New York, pp. 815–841.

Hiesinger, H., Marchi, S., Schmedemann, N., Schenk, P., Pasckert, J.H., Neesemann, A., O'Brien, D.P., Kneissl, T., Ermakov, A.I., Fu, R.R., Bland, M.T., Nathues, A., Platz, T., Williams, D.A., Jaumann, R., Castillo-Rogez, J.C., Ruesch, O., Schmidt, B., Park, R.S., Preusker, F., Buczkowski, D.L., Russell, C.T., Raymond, C.A., 2016. Cratering on Ceres: implications for its crust and evolution. Science 353, 6303. https://doi.org/10.1126/science.aaf4759.

Holmes, W., Hopkins, D., Foster, H., 1968. Pingos in central alaska. U.S. Geol. Survey Bull. 1241-H, 39.

Kenkmann, T., 2002. Folding within seconds. Geology 30, 231–234.

Keil, K., Stoffler, D., Love, S., Scott, E., 1997. Constraints on the role of impact heating and melting in asteroids. Met. Planet. Sci. 32, 349–363.

Konopliv, A., Park, R.S., Vaughan, A.T., Bills, B.G., Asmar, S.W., Ermakov, A.I., Rambaux, N., Raymond, C.A., Castillo-Rogez, J.C., Russell, C.T., Smith, D.E., Zuber, M.T., 2018. The Ceres gravity field, spin pole, rotation period and orbit from the Dawn radiometric tracking and optical data. Icarus 299, 411–429. https://doi.org/10.1016/j.icarus.2017.08.005.

Kueppers, M., 12 others, 2014. Localized sources of water vapour on the dwarf planet (1) Ceres. Nature 505, 525–527 doi:10.1038.

Mackay, J.R., 1998. Pingo Growth and collapse, Tuktoyaktuk Peninsula Area, Western Arctic Coast, Canada: a long-term field study, Geog. Physique et Quatr. 52, 1–53.

McCord, T., Sotin, C., 2005. Ceres: evolution and current state. J. Geophys. Res. 110, E05009. https://doi.org/10.1029/2004JE002244.

Melosh, H.J., 1982. A schematic model of crater modification by gravity. J. Geophys Res. 87, 371–380.

Milton, D.J., Barlow, B.C., Brett, R., Brown, A.R., Glikson, A.Y., Manwaring, E.A., Moss, F.J., Sedmik, E.C.E., Van Son, J., Young, G.A., 1972. Gosses Bluff impact structure, Australia. Science 175, 1199–1207.
Moore, J.M., Malin, M.C., 1988. Dome craters on Ganymede. Geophys. Res. Lett. 15, 225–228.
Nathues, A., Hoffman, M., Platz, T., Thangjam, G.S., Cloutis, E.A., Reddy, V., Le Corre, L., Li, J.-Y., Mengel, K., Rivkin, A., Applin, D.M., Schaefer, M., Christensen, U., Sierks, H., Ripken, J., Schmidt, B.E., Hiesinger, H., Sykes, M.V., Sizemore, H.G., Preusker, F., Russell, C.T., 2016. FC colour images of dwarf planet Ceres reveal a complicated geological history. P&SS 134, 122–127. https://doi.org/10.1016/j.pss.2016.10.017.
Nathues, A., Platz, T., Thangjam, G., Hoffmann, M., Scully, J., Stein, M., Ruesch, O., Mengel, K., 2018. Occator Crater in Color at Highest Spatial Resolution. Icarus, This Issue. in press.
Neesemann, A., and 12 others, The various ages of Occator crater, Ceres: Results of a comprehensive synthesis approach, Icarus, this issue, in press.
Onorato, P.I.K., Uhlmann, D.R., Simonds, C.H., 1978. The thermal history of the Manicouagan impact melt sheet, Quebec. J. Geophys. Res. 83, 2789–2798.
Osinski, G.R., Tornabene, L.L., Banerjee, N.R., Cockell, C.S., Flemming, R., Izawa, M.R.M., McCutcheon, J., Parnell, J., Preston, L., Pickersgill, A.E., Pontefract, A., Sapers, H.M., Southam, G., 2013. Impact-generated hydrothermal systems on Earth and Mars. Icarus 224, 347–363.
Passey, Q.R., Shoemaker, E.M., 1982. Craters and Basins on Ganymede and Callisto: Morphological indicators of Crustal Evolution. In: Morrison, D. (Ed.), Satellites of Jupiter. Univ. of Arizona Press, Tucson, pp. 340–378.
Park, R., Konopliv, A.S., Bills, B.G., Rambaux, N., Castillo-Rogez, J.C., Raymond, C.A., Vaughan, A.T., Ermakov, A.I., Zuber, M.T., Fu, R.R., Toplis, M.J., Russell, C.T., Nathues, A., Preusker, F., 2016. A partially differentiated interior for (1) Ceres deduced from its gravity field and shape. Nature 537 (7621), 515–517. https://doi.org/10.1038/nature18955.
Pike, R.J., 1980. Control of crater morphology by gravity and target type: Mars, Earth, Moon. In: Proc. Lunar Planet Sci. Conf., 11th, pp. 2159–2189.
Prettyman, T.H., Yamashita, N., Toplis, M.J., McSween, H.Y., Schorghofer, N., Marchi, S., Feldman, W.C., Castillo-Rogez, J., Forni, O., Lawrence, D.J., Ammannito, E., Ehlmann, B.L., Sizemore, H.G., Joy, S.P., Polanskey, C.A., Rayman, M.D., Raymond, C.A., Russell, C.T., 2016. Extensive water ice within Ceres aqueously altered regolith: evidence from nuclear spectroscopy. Science 6765, 1–11. https://doi.org/10.1126/science.aah6765.
Preusker, F., et al., 2016. Dawn at Ceres – Shape models and rotational state. In: Lunar Planet. Sci. Conf. 47, pp. 1954.
Quick, L., Buczkowski D., Ruesch O., Scully J., Castillo-Rogez J., Raymond C., Schenk P., Sizemore H., Sykes M., 2018. A Possible Brine Reservoir Beneath Occator Crater: Thermal and Compositional Evolution and Formation of the Cerealia Dome and Vinalia Faculae, Icarus, this issue, in press.
Raponi, A., De Sanctis M.C., Carrozzo F.G., Ciarniello M., Castillo-Rogez J.C., Ammannito E., Frigeri A., Longobardo A., Palomba E., Tosi F., Zambon F., Raymond C.A., Russell C.T., 2018. Mineralogy of Occator crater on Ceres, this issue.
Ruesch, O., Platz, T., Schenk, P., McFadden, L.A., Castillo-Rogez, J.C., Quick, L.C., Byrne, S., Preusker, F., O'Brien, D.P., Schmedemann, N., Williams, D.A., Li, J.-Y., Bland, M.T., Hiesinger, H., Kneissl, T., Neesemann, A., Schaefer, M., Pasckert, J.H., Schmidt, B.E., Buczkowski, D.L., Sykes, M.V., Nathues, A., Roatsch, T., Hoffmann, M., Raymond, C.A., Russell, C.T., 2016. Cryovolcanism on Ceres. Science 353, 6303. https://doi.org/10.1126/science.aaf4286.
Ruesch, O., Quick, L. C., Landis, M., Sori, M., Cadek, O; Broz, K., Otto, K., Bland, M. T., Byrne, S., Castillo-Rogez, J. C., Hiesinger, H., Jaumann, R., Krohn, K., McFadden, L. A., Nathues, A., Neesemann, A., Preusker, F., Roatsch, T., Schenk, P. M., Scully, J., Sykes, M. V., Williams, D. A., Raymond, C. A., Russell, C. T., 2018. Bright Carbonate Surfaces on Ceres as Remnants of Salt-Rich Water Fountains. Icarus, this issue, in press.
Russell, C., Raymond, C.A., Ammannito, E., Buczkowski, D.L., DeSanctis, M.C., Hiesinger, H., Jaumann, R., Konopliv, A.S., McSween, H.Y., Nathues, A., Park, R.S., Pieters, C.M., Prettyman, T.H., McCord, T.B., McFadden, L.A., Mottola, S., Zuber, M.T., Joy, S.P., Polanskey, C., Rayman, M.D., Castillo-Rogez, J.C., Chi, P.J., Combe, J.P., Ermakov, A., Fu, R.R., Hoffmann, M., Jia, Y.D., King, S.D., Lawrence, D.J., Li, J.-Y., Marchi, S., Preusker, F., Roatsch, T., Ruesch, O., Schenk, P., Villarreal, M.N., Yamashita, N., 2016. Dawn arrives at Ceres: exploration of a small, volatile-rich world. Science 353 (6303), 1008–1010. https://doi.org/10.1126/science.aaf4219.
Schenk, P.M., 1989. Crater formation and modification on the icy satellites of Uranus & Saturn: depth/diameter & central peak occurrence. J. Geophys. Res. 94, 3812–3832.
Schenk, P.M., 1991. Ganymede and Callisto: complex crater morphology and formation processes on icy satellites. J. Geophys. Res. 96 (15), 635 15,664.
Schenk, P.M., 1993. Central pit and dome craters: exposing the interiors of Ganymede and Callisto. J. Geophys. Res. 98, 7475–7498.
Schenk, P., Chapman, C., Zahnle, K., Moore, J., 2004. Ages and *interiors: the cratering record of the Galilean satellites*. Jupiter. Cambridge Press, pp. 427–456.
Schenk, P., 18 others, 2016. Impact cratering on the small planets Ceres and Vesta: S-C transitions, central pits, and the origin of bright spots. In: Lunar Planet. Sci. Conf. 47th, abstr. No. 1903.
Schenk, P., White, O., Byrne, P., Moore, J., 2018. Geology of Saturn's *other* Icy Moons. Enceladus and the Icy Moons of Saturn. Univ. Ariz. Press in press.
Schubert, G., Anderson, J., Spohn, T., McKinnon, W., 2004. Interior composition, *structure and dynamics* of the Galilean *satellites*. Jupiter. Cambridge Press, pp. 281–306.
Schmidt, B., Hughson, K.H.G., Chilton, H.T., Scully, J.E.C., Platz, T., Nathues, A., Sizemore, H., Bland, M.T., Byrne, S., Marchi, S., O'Brien, D.P., Schorghofer, N., Hiesinger, H., Jaumann, R., Pasckert, J.H., Lawrence, J.D., Buczkowski, D., Castillo-Rogez, J.C., Sykes, M.V., Schenk, P.M., DeSanctis, M.-C., Mitri, G., Formisano, M., Li, J.-Y., Reddy, V., LeCorre, L., Russell, C.T., Raymond, C.A., 2017. Geomorphological evidence for ground ice on dwarf planet Ceres. Nat. Geosci. 10 (5), 338–343. https://doi.org/10.1038/ngeo2936.
Scully, J., Buczkowski D., Raymond C., Bowling T., Williams D., Neesemann A., Schenk P., Castillo-Rogez J., Russell C., 2018. Ceres' Occator Crater and its Faculae Explored Through Geologic Mapping, Icarus, this issue, in press.
Senft, L.E., Stewart, S.T., 2011. Modeling the morphological diversity of impact craters on icy satellites. Icarus 214, 67–81.
Simonds, C.H., Warner, J.L., Phinney, W.C., McGee, P.E., 1976. Thermal model for impact melt lithification: Manicouagan and the Moon. In: Proc. Lunar Planet. Sci. Conf. 7. pp. 2509–2528.
Sizemore, H.G., Platz, T., Schorghofer, N., Prettyman, T.H., De Sanctis, M.C., Crown, D.A., Schmedemann, N., Neesemann, A., Kneissl, T., Marchi, S., Schenk, P.M., Bland, M.T., Schmidt, B.E., Hughson, K.H.G., Tosi, F., Zambon, F., Mest, S.C., Yingst, R.A., Williams, D.A., Russell, C.T., Raymond, C.A., 2017. Pitted terrains on (1) Ceres and implications for shallow subsurface volatile distribution. Geophys. Res. Lett. 44, 6570–6578. https://doi.org/10.1002/2017GL073970.
Sori, M., Byrne, S., Bland, M.T., Bramson, A.M., Ermakov, A.I., Hamilton, C.W., Otto, K.A., Ruesh, O., Russell, C.T., 2017. The vanishing cryovolcanoes of Ceres. Geophys. Res. Lett. 44, 1243–1250. https://doi.org/10.1002/2016GL0772319.
Stein, N., Ehlmann, B. L., Palomba, E., De Sanctis, M. C., Nathues, A., Hiesinger, H., Ammannito, E., Raymond, C. A., Jaumann, R., Longobardo, A., Russell, C. T., 2018. The Formation and Evolution of Bright Spots on Ceres. Icarus, this issue, in press.
Tornabene, L., 2012. Widespread crater-related pitted materials on Mars: further evidence for the role of target volatiles during the impact process. Icarus 220, 348–368.
Villarreal, M., Russell, C.T., Luhmann, J.G., Thompson, W.T., Prettyman, T.H., A'Hearn, M.F., Kuppers, M., O'Rourke, L., Raymond, C.A., 2017. The dependence of the Cerean exosphere on solar energetic particle events. Astrophys. J. 838, 1.
White, O.L, Schenk, P.M., Dombard, A.J., 2013. Impact basin relaxation on Rhea and Iapetus and relation to past heat flow. Icarus 223, 699–709.
White, O.L., Schenk, P.M., Bellagamba, A., Grimm, A., Dombard, A.J., Bray, V., 2017. Impact crater relaxation on *Dione* and *Tethys* and relation to past heat flow. Icarus 288, 27–52.
Williams, N., Bell, J., Christiansen, P., Farmer, J., 2015. Evidence for an explosive origin for central pit craters on Mars. Icarus 252, 175–185.
Wilshire, H.G., Offield, T.W., Howard, K.A., Cummings, D., 1972. Geology of the Sierra Madera Cryptoexplosion Structure, Pecos County, Texas. U.S. Geol. Surv. Prof. Pap. 599-H. pp. 42.
Wilson, C.W., Stearns, R.G., 1968. Geology of the Wells Creek structure, Tennessee. Tenn. Div. Geol. Bull. 68, 236.
Wolaver, B., Keppel M., Love A., 2013. Hydrogeology of Dalhousie springs, in Allocating Water and Maintaining Springs in the Great Artesian Basin, Volume III: Groundwater Discharge of the Western Great Artesian Basin, Eds., A. J. Love, P. Shand, L. J. Crossey, G. A. Harrington, P. Rousseau-Gueutin, pp.81–99.
Wood, C.A., Head, J., Cintala, M., 1978. Interior morphology of fresh Martian craters - the effects of target characteristics. In: Proc. Lunar Planet. Sci. Conf. IX, pp. 3691–3709.
Xiao, Z., Zeng, Z., Komatsu, G., 2014. A global inventory of central pit craters on the Moon: distribution, morphology and geometry. Icarus 227, 195–201.
Yin, H., Grossing, R., 2006. Balancing and restoration of pier cement structures: geologic insights from 3D kinematic models. J. Struct. Geol. 28, 99–114.
Zolotov, M., 2017. Aqueous origins of bright salt deposits on Ceres. Icarus 296, 289–304.